

## Removal of Acid Yellow 11 dye using a novel modified biochar derived from watermelon peels

Mohamed A. El Nemr<sup>a</sup>, Nabil M. Abdelmonem<sup>a</sup>, Ibrahim M.A. Ismail<sup>a,b</sup>, Safaa Ragab<sup>c</sup>, Ahmed El-Nemr<sup>c,\*</sup>

<sup>a</sup>Department of Chemical Engineering, Faculty of Engineering, Cairo University, Giza, Egypt

<sup>b</sup>Renewable Energy Program, Zewail City of Science and Technology, Egypt

<sup>c</sup>Environmental Division, National Institute of Oceanography and Fisheries, Kayet Bey, El-Anfoushy, Alexandria, Egypt, emails: ahmedmoustafaelnemr@yahoo.com/ahmed.m.elnemr@gmail.com (A. El Nemr)

Received 2 February 2020; Accepted 5 June 2020

---

### ABSTRACT

Acid Yellow 11 (AY11) dye is one of many industries used organic dyes which has a harmful effect for aquatic life. In this work, the biochar prepared from watermelon peels and modified with ozone, ammonium hydroxide, and triethylenetetramine was tested as adsorbents for AY11 dye. The influences of different process parameters on the adsorption of AY11 dye onto watermelon peel biochars were examined in batch experiments. On the other hand, the effect of the modification methods on the efficiency of biochar was studied using isotherm and kinetic models. Chemical, thermal, and surface characteristics of raw watermelon peel and its biochars were determined by Fourier-transform infrared spectroscopy, thermogravimetric analysis, differential thermal analysis, differential scanning calorimetry, scanning electron microscopy, Brunauer–Emmett–Teller and energy-dispersive X-ray spectroscopy analysis. The amounts of AY11 dye adsorbed at equilibrium ( $q_e$ ) onto prepared watermelon biochars were ranged between 76.94 and 462.18 mg g<sup>-1</sup> at pH 1.0 after 180 min contact time at room temperature. The percentages of removal of AY11 dye were found to be >96%. The Freundlich and Langmuir isotherm was the best fitting isotherm model for the adsorption process and the adsorption rate was primarily controlled by the pseudo-second-order model.

*Keywords:* Acid Yellow 11 dye; Watermelon peel; Biochar; Water treatment; Removal

---

### 1. Introduction

Polluted water is a major environmental problem and is one of the leading worldwide cause of death and diseases [1,2]. Some industrial facilities generate large volumes of wastewater and have been failed at redesigning their manufacturing processes to reduce or eliminate pollutants [3]. This wastewater contains different organic pollutants. They are pesticides, industrial chemicals, or unwanted by-products of industrial processes and dyes. Nowadays, about 100,000 synthetic dyes are used commercially and 700,000 tons of dye is produced annually [4]. Textile dyes

are one of the major groups of organic pollutants that impose an increasing environmental danger. Up to 20% of the total world production of dyes is lost during the dyeing process and is discharged into the environment [3,5]. The wastewater containing textile dyes are mostly toxic to various microorganisms, aquatic life, and human being even at very low concentrations due to their negative eco-toxicological effects, bioaccumulation in wildlife and generates toxic by-products which may be many times more toxic to the environment than the parent compound as a result of many chemical reactions taking place in the wastewater phase [6]. Dyes color the water sources and damage living organisms

---

\* Corresponding author.

by ceasing the oxygenation ability of water, arresting sunlight, and therefore, natural growth activity of aquatic life is disturbed [2]. The textile industry is the largest consumer of high-quality freshwater per kg of treated material [7]. It is necessary to treat and remove these toxic effluents which are found in wastewaters prior to their discharge into the receiving water. There are several traditional methods for the treatment of dyes from wastewater. Various techniques are often applied, such as photocatalytic degradation [8–11], chemical precipitation [12], chemical coagulation followed by sedimentation [13], ion exchange [14], ultrafiltration [15], physical adsorption [16–19], electrochemical degradation [20], bio-removal [21], adsorption/precipitation [22], integrated chemical/biological degradation [23], solar photo-Fenton process [11,24], and biological process [25]. Also, there are other advanced techniques such as UV, ozonation, ultrasonic decomposition, or combined oxidation processes [26–31]. Amongst these various techniques of dye treatment, adsorption is the best choice because of their easy handling, economic feasibility, simplicity in design, and produce a high-quality treated effluent [32]. Also, the gamma radiation-induced degradation of congo-red dye [33] and partially exfoliated graphite for organic dyes removal were studied [34]. Gum Arabic-crosslinked poly(acrylamide)/Ni(OH)<sub>2</sub>/FeOOH nanocomposites hydrogel [35] and monometallic and bimetallic quantum dots based nanocomposites were used for photodegradation of toxic dye [36]. Biochar is a charcoal-like substance that's made by burning organic material from agricultural and forestry wastes in a controlled process called pyrolysis. Biochar is a fine-grained and porous substance and has been applied recently to remove dyes from aqueous solutions [37–39]. The biochar adsorption capacity has a direct relation with biochar physiochemical properties such as surface area, pore size distribution, functional groups on the surface, and cation exchange capacity, while physicochemical properties vary with the preparation conditions [40–42]. The physicochemical properties of biochar may be improved with acids, alkali, and oxidizing agents [43]. Acid Yellow 11 (AY11) dye-containing a single azo class was selected as a model for the anionic dye, which could cause more serious problems as the dyes are discharged into the environment. AY11 dye mainly applied for wool, silk, polyamide fiber, and leather dyeing besides its use in painting, medicine, paper surface, and cosmetics of shading. Modernity in this work is the use of watermelon peels in the preparation of biochar for the first time and then treating biochar produced with ozone followed by ammonium hydroxide to form amine groups on the surface of biochar to increase its ability to absorb dyes from water. The high nitrogen content introduced into the new biochar prepared from watermelon peels as a worthless waste has resulted in the production of new good quality materials that have a great ability to absorb dyes from water.

In this study, the first objective was to investigate the adsorption behavior of unmodified and modified watermelon peels biochar for the removal of the anionic AY11 dye at room temperature. The second objective was to evaluate the effect of surface functionalization on the adsorption process of anionic AY11 dye. The surface of the biochars was functionalized and modified by using ozone gas in the presence of water, and then the biochar surface is modified by

boiling with ammonia or triethylenetetramine to introduce nitrogen to the biochar surface to increase the efficiency of the biochar as adsorbent. Various instrumental techniques such as Fourier-transform infrared spectroscopy (FTIR), thermogravimetric analysis (TGA), differential thermal analysis (DTA), differential scanning calorimetry (DSC), scanning electron microscopy (SEM), Brunauer–Emmett–Teller (BET) and energy-dispersive X-ray spectroscopy (EDAX) analysis were employed to reveal the surface chemistry. Different isotherm and kinetic models were used to analyze the AY11 dye removal process.

## 2. Materials and methods

Acid Yellow 11 (AY11) dye (C.I. 18820) (C<sub>16</sub>H<sub>13</sub>N<sub>4</sub>O<sub>4</sub>Na) (Mwt = 380.35 g) used in this study was purchased from Sigma-Aldrich (USA), which was of analytical grade and it was used without further purification. Raw bio-sorbent watermelon peel was obtained from a local market. Ammonia solution (NH<sub>4</sub>OH, M.W. = 35 g, assay 25%), triethylenetetramine (TETA), and sulfuric acid (H<sub>2</sub>SO<sub>4</sub>, M.W. = 98.07 g, assay (acid-metric) 99%) were obtained from Sigma-Aldrich (USA).

### 2.1. Adsorbate preparation

A stock solution of AY11 dye with a concentration of 1,000 mg L<sup>-1</sup> was prepared and dilutions were made with doubly distilled water to make different concentrations. The residual AY11 concentration of all the solutions was measured on a UV-visible spectrophotometer at adsorption wavelength of 1<sub>407</sub> nm (SPEKOL 1300, Analytic Jena (EU), wavelength range 100–1,000 nm). The solutions were shaken with different doses of the prepared adsorbent in a shaker (JSOS-500, Korea), then filtered, and the remaining color was measured. The adsorption capacities of adsorbents and the removal percentage of AY11 dye from aqueous were calculated using Eqs. (1) and (2), respectively.

$$q_t = \frac{(C_0 - C_t)}{w} \times V \quad (1)$$

$$\text{Removal (\%)} = \frac{(C_0 - C_t)}{C_0} \times 100 \quad (2)$$

where  $q_t$  is the adsorption capacity of the adsorbent at time  $t$  (mg adsorbate/g adsorbent);  $C_0$  is the initial concentration of dye (mg L<sup>-1</sup>);  $C_t$  is the residual concentration of the dye after adsorption had taken place over a period time  $t$  (mg L<sup>-1</sup>);  $V$  (L) is the volume in liter of dye solution and  $W$  (g) is mass of adsorbent in gram.

### 2.2. Preparation and modification of biochar

Watermelon peels were washed with tap water to remove any water-soluble impurities and adhering dirt. After washing, watermelon peels were dried at 105°C for 48 h and crushed to particles using an electric grinder. The crushed melon peels were boiled in a refluxed system using 25 g in a 100 mL solution of 50% H<sub>2</sub>SO<sub>4</sub> for 2 h then the samples were filtered and repeatedly washed with distilled water until

the filtrate reached a neutral pH followed by washing with ethanol. The particles were then dried at 70°C for 24 h, and then its weight is determined. The obtained biochar from this reaction was labeled as Melon-B. In this preparation method, the carbonization and sulfonation processes occurred. The yield of biochar is calculated as a percentage weight of the resultant biochar divided by the weight of watermelon peel as in the following Eq. (3):

$$\text{Yield of biochar \%} = \frac{\text{Weight to biochar}}{\text{Weight of dried Pea or melon peels}} \times 100 \quad (3)$$

In this work, the prepared Melon-B biochar was subsequently subjected to two stages of modification. The Melon-B biochar was oxidized using ozone as an oxidant in water for 2 h. After the oxidation process, the samples of activated biochar by ozone were filtered and washed by distilled water, ethanol, and then dried in an oven overnight at 70°C. The modified samples were referred to as Melon-BO biochar. Oxidation by ozone was urgent to make the oxidation of the biochar surface to increase the oxygen-containing functional groups such as –OH, –COOH, etc. Then, chemical reduction known as the alkali modification method and also can improve porosity and specific surface area of biochar. The adsorption capacity of biochar for pollutants is enhanced. Two amine-functionalized biochars were obtained by using different reducing agents [triethylenetetramine (TETA) and ammonium hydroxide (NH<sub>4</sub>OH)]. For functionalized biochar with NH<sub>4</sub>OH, 25 g of as-prepared Melon-BO biochar was boiled in a refluxing system using 100 mL solution of 25% NH<sub>4</sub>OH or TETA for 2 h, followed by filtration, then washed with distilled water and ethanol. Finally, the amine-functionalized Melon-BO-NH<sub>2</sub> biochar was dried in the oven at 70°C for 24 h, and then its weight is determined. The product was labeled as Melon-BO-NH<sub>2</sub> or Melon-BO-TETA biochar, respectively.

### 2.3. Characterization of adsorbent biochar

The adsorption–desorption isotherm of nitrogen gas on biochar was determined at the boiling point of N<sub>2</sub> gas. The BET surface area ( $S_{\text{BET}}$ ) measurements of the biochar were made by nitrogen adsorption at 77 K using surface area and pore analyzer (BELSORP-Mini II, BEL Japan, Inc., Japan) [44,45]. Analysis of the isotherm was carried out by applying the BET plot to obtain monolayer volume ( $V_m$ ) (cm<sup>3</sup> (STP) g<sup>-1</sup>), the surface area ( $S_{\text{BET}}$ ) (m<sup>2</sup> g<sup>-1</sup>), total pore volume ( $V_T$ ) ( $p/p_0$ ) (cm<sup>3</sup> g<sup>-1</sup>), (C) energy constant and mean pore diameter (nm). The average pore radius was calculated by using the following Eq. (4).

$$r(\text{nm}) = \frac{2V_T (\text{mL g}^{-1})}{a_{s,\text{BET}} (\text{m}^2 \text{g}^{-1})} \times 100 \quad (4)$$

Also, the micropore surface area ( $S_{\text{mi}}$ ) and micropore volume ( $V_{\text{mi}}$ ), as well as the mesopore surface area ( $S_{\text{mes}}$ ) and mesopore volume ( $V_{\text{mes}}$ ) of biochar, were determined by the

Barrett–Joyner–Halenda (BJH) methods [46], respectively, according to BELSORP analysis program software. Pore size distribution is calculated from desorption isotherm by applying the BJH method [42].

The surface morphology of the biochar samples was analyzed by the scanning electron microscope (QUANTA 250, Czech) which was coupled with an energy-dispersive X-ray spectrometer to carry out an elemental analysis.

The surface functional groups of the biochar were estimated by FTIR spectroscopy (platinum ATR) model V-100 VERTEX 70 (Germany) to detect the infrared-observable functional groups on the biochar surface, in the wavenumber (400–4,000 cm<sup>-1</sup>).

Thermal analyses were performed using an SDT650-simultaneous thermal analyzer instrument (USA) in the range from room temperature to 900°C using 5°C/min as ramping temperature.

### 2.4. Batch adsorption experiments

To determine the applicability of produced unmodified and modified watermelon peels biochar as an adsorbent for water treatment, the batch adsorption experiments were performed using AY11 dye as the adsorbate. The dye stock solution was prepared as mentioned above. Batch equilibrium adsorption studies were performed using 100 mL of dye solutions. Parameters affecting the adsorption process such as pH (1–10), adsorbent dosage (0.5–6.0 g L<sup>-1</sup>), initial dye concentration (75–300 mg L<sup>-1</sup>), contact time (5–180 min) and temperature (25°C) were studied in a batch system. The solutions pH was controlled by solutions of 0.1 M HCl and 0.1 M NaOH. The reaction mixtures were agitated at room temperature using shaker adjusted at 200 rpm. At predetermined time intervals, samples were collected, filtered using a very small piece of glass wool in Pasteur tube to have 2 mL of sample and analyzed by a UV-visible spectrophotometer.

## 3. Results and discussion

### 3.1. Morphological, textural properties and thermal behaviors of biochars

To determine the surface morphology of the raw watermelon peels, unmodified, and modified biochars, SEM analysis was used. SEM photographs for raw watermelon peel, Melon-B, Melon-BO, Melon-BO-NH<sub>2</sub> and Melon-BO-TETA biochars shown in Figs. 1a–e. As shown in Fig. 1b, the Melon-B biochar appears clean and free of any particulate impurities. No evidence of any damage to the pores of the raw watermelon peel as a result of sulfuric acid treatment was observed. The acid treatment did not appear to drastically alter the morphology of the raw watermelon peel. Figs. 1b and c show that a little porosity existed at both Melon-B and Melon-BO biochars which reflects the small surface area for Melon-B and Melon-BO biochars. SEM images of Melon-BO-NH<sub>2</sub> and Melon-BO-TETA biochars are given in Figs. 1d and e, respectively. It is obvious that wider porosity and pores of different sizes are created, thus the surface areas of the modified biochars increased and pore diameter decreased.

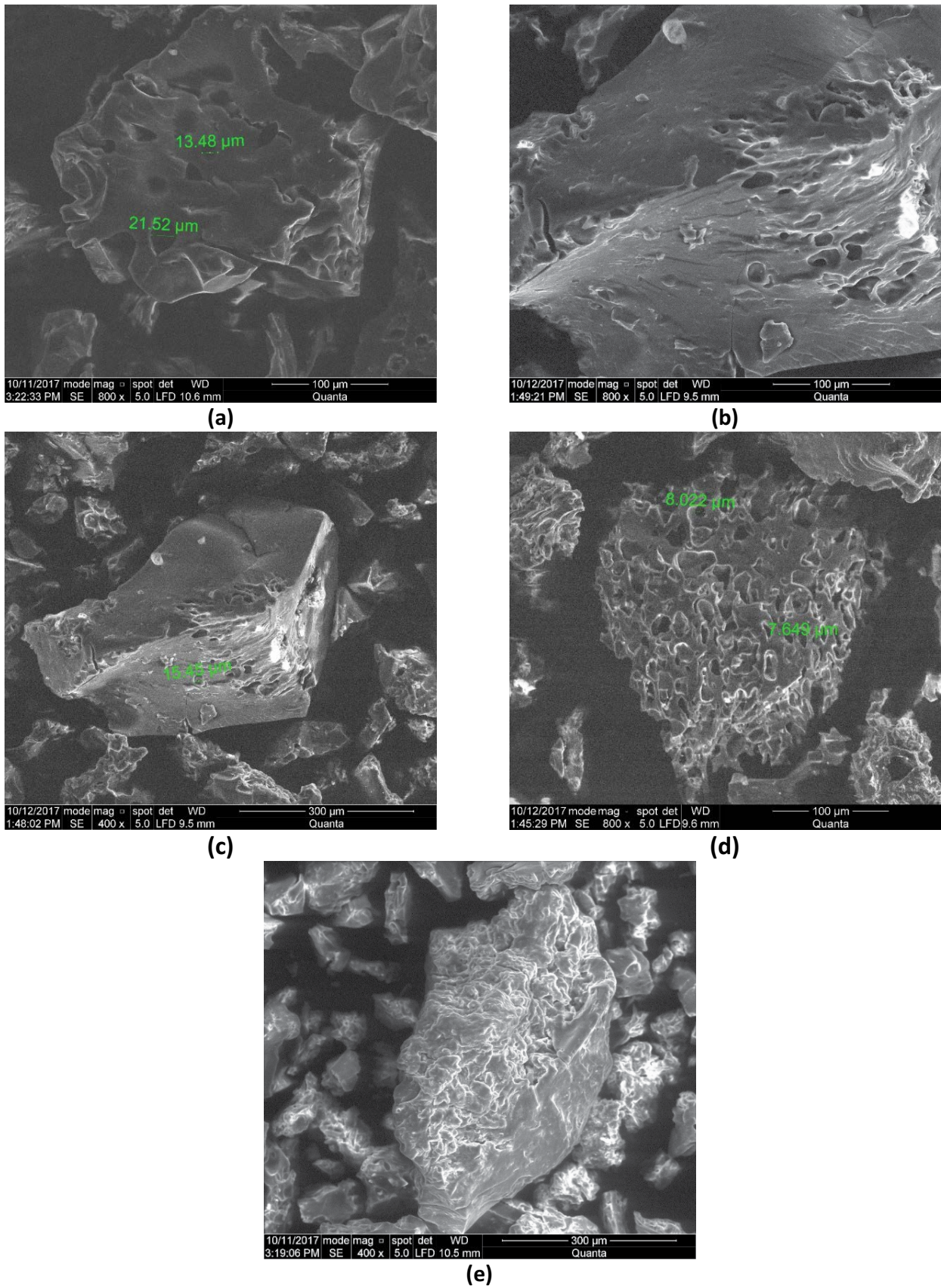


Fig. 1. SEM image of Melon-Peel (a), Melon-B (b), Melon-BO (c), Melon-BO-NH<sub>2</sub> (d), and Melon-BO-TETA (e).

Table 1  
EDAX analysis data of Melon-B, Melon-BO, Melon-BO-NH<sub>2</sub>, and Melon-BO-TETA biochars

Biochar	Melon-B		Melon-BO		Melon-BO-NH <sub>2</sub>		Melon-BO-TETA	
	Wt.%	At.%	Wt.%	At.%	Wt.%	At.%	Wt.%	At.%
C	47.12	64.80	68.32	75.16	59.28	65.68	61.52	66.99
N	ND	ND	ND	ND	13.36	12.70	19.56	18.26
O	14.58	15.01	28.48	23.52	24.88	20.70	17.15	14.02
Al	0.56	0.27	0.56	0.27	ND	ND	0.16	0.08
Si	0.55	0.26	0.55	0.26	ND	ND	0.28	0.13
S	32.9	16.90	1.12	0.46	1.20	0.50	1.14	0.46
K	3.79	1.59	0.45	0.15	ND	ND	ND	ND
Ca	0.51	0.17	0.51	0.17	0.42	0.02	0.19	0.06

ND: not detected.

The nitrogen adsorption–desorption isotherms of the biochars prepared from melon peel were investigated to study the influence of the O<sub>3</sub>, NH<sub>4</sub>OH, and TETA reagents on the surface characteristics. The specific surface area and mesopore area were calculated by the BET and BJH methods. The textural properties including the BET specific surface area, total pore volume, mean pore diameter, monolayer volume, mesopore area, mesopore volume, and mesopore distribution peak for the Melon-B, Melon-BO, and amine-modified (Melon-BO-NH<sub>2</sub> and Melon-BO-TETA) biochars are presented in Fig. S1. The textural properties varied widely among these biochars. In general the BET specific surface area of biochars declined as Melon-BO-NH<sub>2</sub> (14.16 m<sup>2</sup> g<sup>-1</sup>) > Melon-BO-TETA (13.64 m<sup>2</sup> g<sup>-1</sup>) > Melon-B (1.79 m<sup>2</sup> g<sup>-1</sup>) > Melon-BO (1.22 m<sup>2</sup> g<sup>-1</sup>). Notably, the modification increased the surface area of Melon-B and Melon-BO biochars. The monolayer volume values of Melon-BO-NH<sub>2</sub>, Melon-BO-TETA, Melon-BO, and Melon-B biochars were 3.24, 3.13, 2.81, and 0.41 cm<sup>3</sup> g<sup>-1</sup>, respectively, which demonstrated a similar trend with the surface area. The total volume values of Melon-B, Melon-BO, Melon-BO-NH<sub>2</sub>, and Melon-BO-TETA biochars were 0.006, 0.017, 0.018, and 0.021 cm<sup>3</sup> g<sup>-1</sup>, respectively. The mean pore diameters of Melon-B, Melon-BO, Melon-BO-NH<sub>2</sub>, and Melon-BO-TETA biochars were 12.47, 5.70, 5.17, and 6.05 nm (mesopores), respectively.

This result revealed that the modification process reduced the pore size of Melon-BO, Melon-BO-NH<sub>2</sub>, and Melon-BO-TETA biochars. The meso-surface area of biochars declined as Melon-BO-TETA (13.49 m<sup>2</sup> g<sup>-1</sup>) > Melon-BO-NH<sub>2</sub> (12.97 m<sup>2</sup> g<sup>-1</sup>) > Melon-BO (11.75 m<sup>2</sup> g<sup>-1</sup>) > Melon-B (1.82 m<sup>2</sup> g<sup>-1</sup>). Notably, the modification increased the surface area of Melon-B biochar. The mesopore volume values of Melon-BO-TETA, Melon-BO-NH<sub>2</sub>, Melon-BO, and Melon-B biochars were 0.023, 0.021, 0.021, and 0.006 cm<sup>3</sup> g<sup>-1</sup>, respectively, which demonstrated a similar trend with the surface area. The mesopore distribution peak values of Melon-B, Melon-BO, Melon-BO-NH<sub>2</sub>, and Melon-BO-TETA biochars were 1.22, 1.66, 1.66, and 1.22 nm, respectively. As expected, the surface area, total pore volume, and monolayer volume were increased via modification due to the evolution of new pores. The mean pore diameter was decreased; this result revealed the modification process controls the morphology of the surface of biochar.

Thermal analysis has been widely used to get knowledge of the thermal behaviors of biochar. TGA was performed on the selected Melon-B biochars in order to detect the influence of their structural differences on the degradation behavior and to define operating temperature. Each sample was heated from room temperature to 1,000°C under N<sub>2</sub> atmosphere. Fig. 2a shows TGA analysis curves related to raw watermelon peel, Melon-B, Melon-BO, Melon-BO-NH<sub>2</sub>, and Melon-BO-TETA biochars. All samples showed their first weight loss peaks before 100°C, which are attributed to the volatilization of the H<sub>2</sub>O molecules. For watermelon peel, Melon-B, and oxidized Melon-BO biochars, the second weight loss peak occurs at above 100°C due to the decomposition of different oxygen functional groups. Strongly acidic functionalities such as carboxylic, anhydrides, and lactones decompose at lower temperatures while weakly acidic functionalities such as phenol decompose at higher temperatures. In the case of amine-modified samples (Melon-BO-NH<sub>2</sub> and Melon-BO-TETA biochars) the second weight loss peaks appeared above 180°C suggesting the beginning decomposition temperatures of the amines filled inside the pores and coated outside the pores. In the temperature range 100°C–450°C, oxidized and amine-modified samples continue to gradually lose weight, whereas watermelon peel and Melon-B biochar exhibit a slight plateau of weight losses. It should be noted that all TGA curves became similar at the temperature above 450°C due to the decomposition of carbon in the biochar structure. At the final temperature 1,000°C, different weight losses with an order of Melon-BO-NH<sub>2</sub> < Melon-BO-TETA < Watermelon peel < Melon-BO < Melon-B and the lose percentages of 27.95%, 38.95%, 39.56%, 40.74%, and 45.12% were obtained, respectively. The weight remained with an order of Watermelon-peel < Melon-B < Melon-BO-TETA < Melon-BO < Melon-BO-NH<sub>2</sub> biochars and the percentages of 12.62%, 14.50%, 48.82%, 50.65%, and 52.80% were obtained which reflect more stability for oxidized and amine-modified samples than raw watermelon peel and Melon-B biochar. DTA curves may be used as a fingerprint for the determination of phase diagrams, heat change measurements, and decomposition in various atmospheres. Fig. 2b shows the DTA of watermelon peel, Melon-B, Melon-BO, Melon-BO-NH<sub>2</sub>, and Melon-BO-TETA biochars.

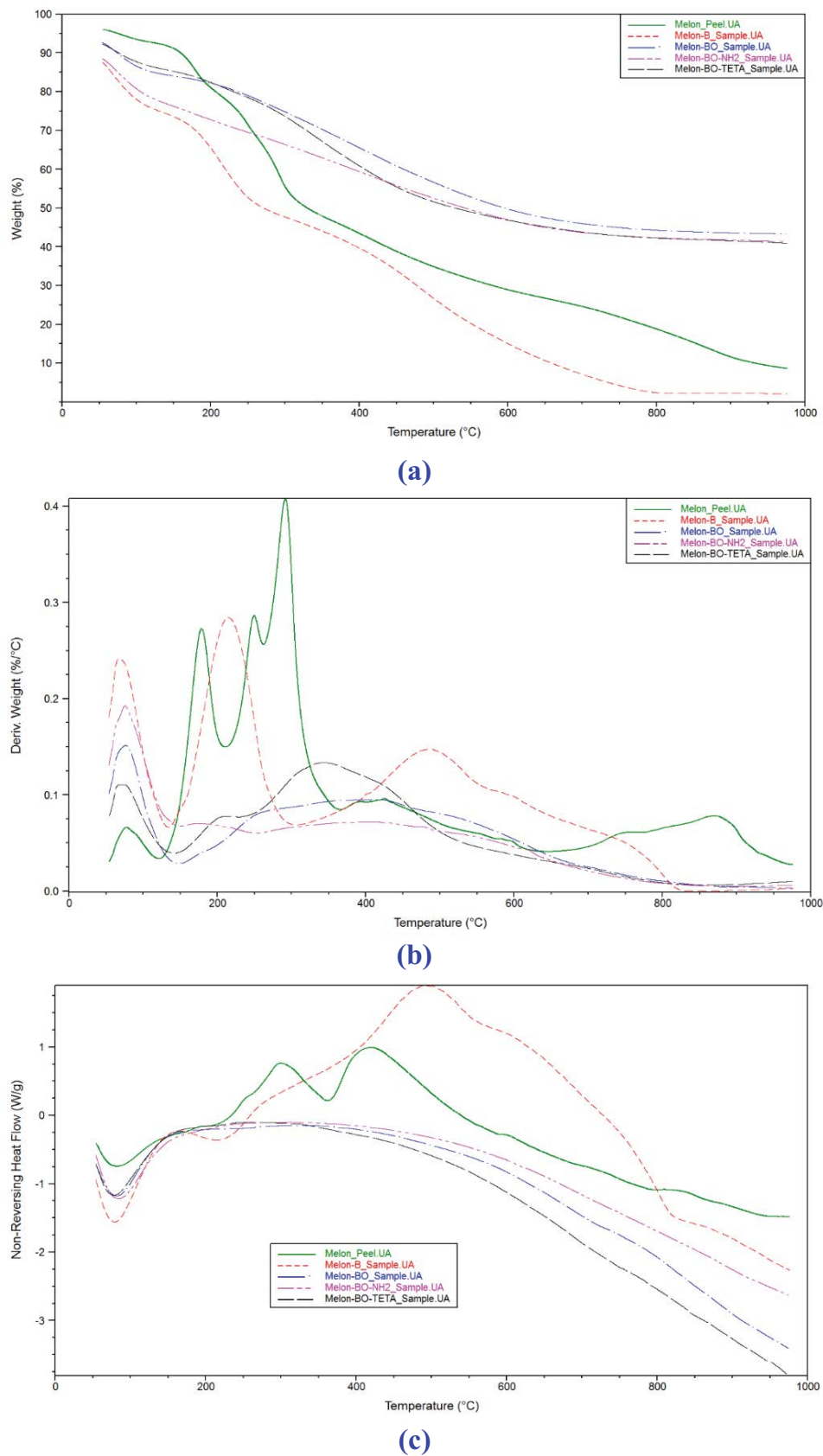


Fig. 2. (a) TGA, (b) DTA, and (c) DSC analyses of watermelon peel and Melon-B, Melon-BO, Melon-BO-NH<sub>2</sub>, and Melon-BO-TETA biochars.

DSC can be utilized to compare materials via thermal transitions. Fig. 2c illustrates the DSC profile of the raw material of melon peel, Melon-B, Melon-BO, Melon-BO-NH<sub>2</sub>, and Melon-BO-TETA biochars, respectively. The DSC was conducted under an N<sub>2</sub> atmosphere with a temperature range from room temperature to 1,000°C. The heating rate of 5°C/min was maintained for all samples. All samples showed their crystallization temperatures  $T_c$  before 100°C which are attributed to crystallization of water molecules except Melon-B showed another crystallization temperatures  $T_c$  at 225.10°C and 818.96°C. Melon-BO, Melon-BO-NH<sub>2</sub>, and Melon-BO-TETA biochars, respectively do not exhibit other phase transitions. As the temperature increased the watermelon peel and Melon-B biochar go through the melting temperature. However, watermelon peel undergoes melting temperatures  $T_m$  at 297.62°C and 422.87°C while Melon-B undergoes melting temperature at 486.76°C. Watermelon peel showed lower transition temperature while Melon-B biochar showed the highest. Higher transition temperatures resulted from a higher degree in crystallinity, which provides structural stability and makes the granules more resistant to gelatinization.

### 3.2. Chemical properties of biochars

The EDAX was used to analyze the chemical composition of the prepared biochars. The elements percent were examined and shown in Table 1. Table 1 had shown the absence of nitrogen before the modification by NH<sub>4</sub>OH or TETA reagents. The EDAX analysis of Melon-BO-NH<sub>2</sub> and Melon-BO-TETA biochars proved the presence of about 13.36% and 19.56% of sample weight for nitrogen element, respectively.

The FTIR spectrum was obtained to evaluate qualitatively the chemical structures of prepared samples before and after modification and is shown in Fig. 3. The watermelon peel was compared with the unmodified melon biochar which was prepared via boiling with H<sub>2</sub>SO<sub>4</sub> (Melon-B) and

also compared with the three modified biochars (Melon-BO, Melon-BO-NH<sub>2</sub>, and Melon-BO-TETA). The spectrum displayed the following bands which indicated various surface functional groups. The spectra of FTIR of all samples demonstrate some similarities. The band at 3,274–3,062 cm<sup>-1</sup> represents the O–H stretching vibration which existed in watermelon peel, Melon-B, and Melon-BO biochars (Fig. 3). The broad adsorption peak around 3,033 and 3,190 cm<sup>-1</sup> is inductive of the existence of the –OH group of glucose and the –NH of the amino group in Melon-BO-NH<sub>2</sub> and Melon-BO-TETA biochars (Fig. 3). These observations indicated that TETA and NH<sub>4</sub>OH were successfully incorporated into biochar structure. The adsorption peak at 2,921 cm<sup>-1</sup> can be assigned to C–H stretching. The strong adsorption peak at 1,702–1,711 cm<sup>-1</sup> can be assigned to C=O stretching of the carboxyl group which was existed in Melon-B and Melon-BO, while it is weak in watermelon peel and it is completely disappeared in Melon-BO-NH<sub>2</sub> and Melon-BO-TETA biochars. However, the strength at 1,702–1,711 cm<sup>-1</sup> of Melon-BO treated biochar was enhanced when compared with watermelon peel or Melon-B biochar, indicating the C=O functional group might be increased by O<sub>3</sub> treatment. The band 1,598–1,601 cm<sup>-1</sup> implies the C=O stretching vibration of β-ketone and almost existed in watermelon peel, Melon-B, and Melon-BO biochars, Fig. 1. The appearance of a new peak at 1,550–1,554 cm<sup>-1</sup> attributed to bending of N–H in fatty amine or aromatic secondary amine in Melon-BO-NH<sub>2</sub> and Melon-BO-TETA biochars. The peak at 1,405–1,418 cm<sup>-1</sup> represents the C–O functional group which was moderate in the melon peel, weak in Melon-B, very weak in Melon-BO while it is completely disappeared in Melon-BO-NH<sub>2</sub> and Melon-BO-TETA biochars, indicating the refluxing in 25% NH<sub>4</sub>OH solution or refluxed in TETA might have a strong effect on the C–O functional group of biochars. Also, the modification leads to the formation of new functional groups, in the FTIR spectra of Melon-BO-NH<sub>2</sub> and Melon-BO-TETA biochar's new peak appeared at 1,354–1,372 cm<sup>-1</sup> and this band attributed to the stretching

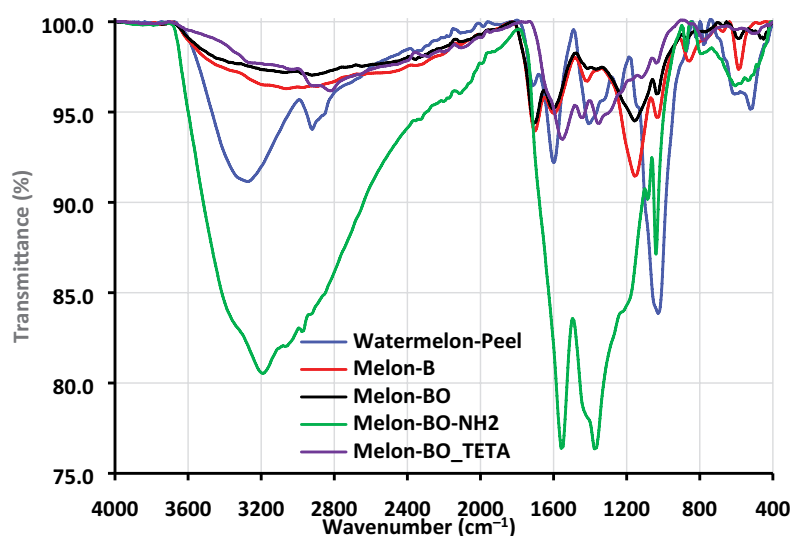


Fig. 3. FTIR analysis of watermelon peel, Melon-B and Melon-BO, Melon-BO-NH<sub>2</sub>, and Melon-BO-TETA.

vibration of  $-N=C=O$  group. These new peaks resulting from nitrogen-containing functional groups appeared on Melon-B biochar, thereby indicating that amino groups were successfully introduced after the treatment. The presence of oxygenated carbon chains peak at  $1,239\text{--}1,084\text{ cm}^{-1}$  represents an increase of C–O–C asymmetric stretching functional group for Melon-B and Melon-BO, while it is very weak in watermelon peel, Melon-BO-NH<sub>2</sub>, and Melon-BO-TETA biochars. The peak at  $1,026\text{--}1,039\text{ cm}^{-1}$  is a primary hydroxyl group which has a strong intensity in watermelon peel and weak intensity in other samples (Fig. 3).

### 3.3. Adsorption of AY11 dye

#### 3.3.1. Effect of pH on the removal of AY11 dye

The pH is an important parameter influencing the removal of dyes since a variation in pH can lead to ionization of the dye molecules or functional groups on the adsorbent [47]. The effect of pH on the removal efficiency and the amounts of AY11 dye adsorbed at equilibrium ( $q_e$ ) (mg g<sup>-1</sup>) by using Melon-B, Melon-BO-NH<sub>2</sub>, and Melon-BO-TETA biochars were studied at varied pH range from 1 to 10 (Fig. 4). In Fig. 4a, the experimental conditions were performed as follows initial concentration of AY11 dye (100 mg L<sup>-1</sup>), adsorbent dose of Melon-B (5.0 g L<sup>-1</sup>), Melon-BO-NH<sub>2</sub> (1.0 g L<sup>-1</sup>) and Melon-BO-TETA (1.0 g L<sup>-1</sup>), contact time (2h) at temperature (25°C ± 2°C). From Fig. 4a, it is observed that the highest efficiency of removal was obtained at pH 1 to be 96%–99%, therefore, the optimum pH value was pH 1. By increasing pH from 1 to 2, the removal percentage of dye is remaining constant, and then the removal percentage of dye is dramatically reduced from 99% to 46% for Melon-B, from 98% to 44% for Melon-BO-NH<sub>2</sub> and from 96% to 42% for Melon-BO-TETA biochars with increasing pH values from 2 to 10.

Fig. 4b shows the relationship between the amounts of AY11 dye adsorbed at equilibrium ( $q_e$ ) (mg g<sup>-1</sup>) and the pH values variation from 1 to 10. The results indicate that,

at different pH values, the  $q_e$  for the Melon-BO-NH<sub>2</sub> and Melon-BO-TETA biochars were nearly similar and the maximum  $q_e$  values were 99 mg g<sup>-1</sup> for Melon-BO-NH<sub>2</sub> and 95 mg g<sup>-1</sup> for Melon-BO-TETA biochars at pH 1. By changing pH values from 2 to 10 the  $q_e$  decreased from 99 to 45 mg g<sup>-1</sup> for Melon-BO-NH<sub>2</sub> and from 95 to 42 mg g<sup>-1</sup> for Melon-BO-TETA. While there was dramatically decreased in  $q_e$  for Melon-B biochar at different pH values. The amount of  $q_e$  for Melon-B biochar at pH 1 was 20 mg g<sup>-1</sup> and highly decreased to 10 mg g<sup>-1</sup> at pH 10. The percentage of removal and the amounts of dye adsorbed at equilibrium were increased five times after oxidation of Melon-B biochar by ozone followed by treatment with NH<sub>4</sub>OH or TETA. The adsorbent doses of Melon-BO-NH<sub>2</sub> and Melon-BO-TETA are five times lower than that of the Melon-B biochars. This dependence of dye uptake on pH may relate to the functional groups of treated biochars. AY11 dye is an anionic dye; its adsorption can be explained on the basis of anionic groups formed during dehydration of watermelon peels by sulfuric acid and also during the treatment of Melon-B biochar by O<sub>3</sub>, NH<sub>4</sub>OH and TETA. It is probable that the amino groups may be formed as a result of the treatment process. The FTIR spectra of raw material and adsorbent treated with O<sub>3</sub>, NH<sub>4</sub>OH and TETA showed that the hydroxyl, carboxyl, and amino groups were increased considerably with the O<sub>3</sub>, NH<sub>4</sub>OH, and TETA treatment, which leads to increase the electrostatic attraction between the dye and biochars. The results indicate that the O<sub>3</sub>, NH<sub>4</sub>OH, and TETA can be used as reagents to modify Melon-B biochar to produce highly efficient adsorbents to remove AY11 dye from water. The percentage of removal of AY11 dye was maximum at acidic pH (1–2) and decreased with further increase in pH values. Lower adsorption of AY11 dye at alkaline pH is due to the presence of an excess of HO<sup>-</sup> ions competing with dye anion for the adsorption sites.

#### 3.3.2. Effect of contact time on the removal of AY11

Equilibrium time is the time which is taken by the adsorbent to adsorb the maximum amount of dye, denoted by  $t$ .

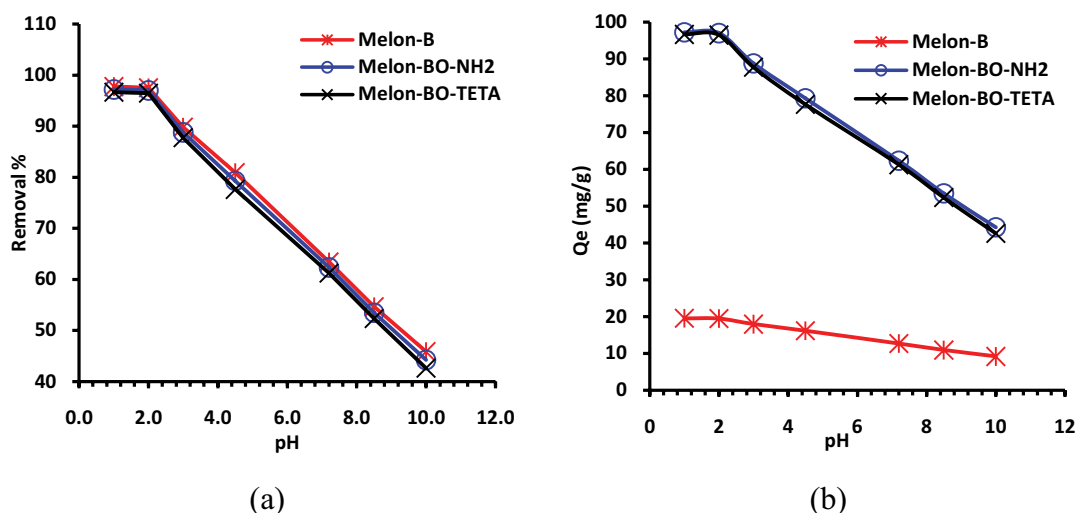


Fig. 4. Effect of solution pH on the (a) removal % and (b)  $q_e$  (mg g<sup>-1</sup>) of AY11 dye (100 mg L<sup>-1</sup>) using Melon-B, Melon-BO-NH<sub>2</sub>, and Melon-BO-TETA of adsorbent dose (5.0, 1.0, and 1.0 g L<sup>-1</sup>, respectively) at 25°C ± 2°C.

The experiments were carried out at initial concentrations of AY11 dye (75, 100, 150, and 200 mg L<sup>-1</sup>) using 2.0 g L<sup>-1</sup> of untreated Melon-B biochar at pH 1.0 and room temperature 25°C ± 2°C. The effect of contact time on the adsorption of AY11 dye on adsorbent concentration is presented in Fig. 5. As can be observed from Fig. 5, within 15 min, the percentage of removal was about 75% at 75 mg L<sup>-1</sup> initial concentration of AY11 dye onto Melon-B adsorbent dose (2.0 g L<sup>-1</sup>), while the removal percentage at 100 mg L<sup>-1</sup> initial concentration of AY11 dye was decreased to 40%. The removal percentage of AY11 dye increases with an increase in time and reaches a maximum of 92% and 80% for 75 and 100 mg L<sup>-1</sup> initial concentration of AY11 dye, respectively. The removal percentage of AY11 dye is about 35% at 150 and 200 mg L<sup>-1</sup> initial concentration of AY11 dye onto 2.0 g L<sup>-1</sup> Melon-B adsorbent dose then the uptake of AY11 dye slightly increased with increase in time until reaches the maximum removal percentage (70%) at equilibrium. The optimum time to attain the equilibrium is 3 h. The removal

of dye by adsorption using Melon-B biochar was found to be rapid at the initial period of contact time and then become slower with the increase of contact time.

Fig. 5b shows the removal percentage of AY11 dye at different initial dye concentrations ranged from 100 to 300 mg L<sup>-1</sup> and pH 1 using Melon-BO-NH<sub>2</sub> adsorbent biochar (2.0 g L<sup>-1</sup>). With the beginning of adsorption, the removal of AY11 dye increases quickly and reaches about 95% within 10 min, most of the AY11 dye is removed and reaches a complete removal at 3 h. The relationship between the removal percentage of AY11 dye using Melon-BO-TETA adsorbent (2.0 g L<sup>-1</sup>) and different contact time was shown in Fig. 5c. It is shown in Fig. 5c that the removal percentage trend of AY11 dye on Melon-BO-TETA biochar for all cases was speedy within the first 15 min. For initial dye concentration of 100 mg L<sup>-1</sup>, the removal of dye was 55% within 15 min, after 60 min the removal became 82% and after that, the removal increased slowly to reach the maximum value 95% after 3 h contact time. The removal for an initial dye

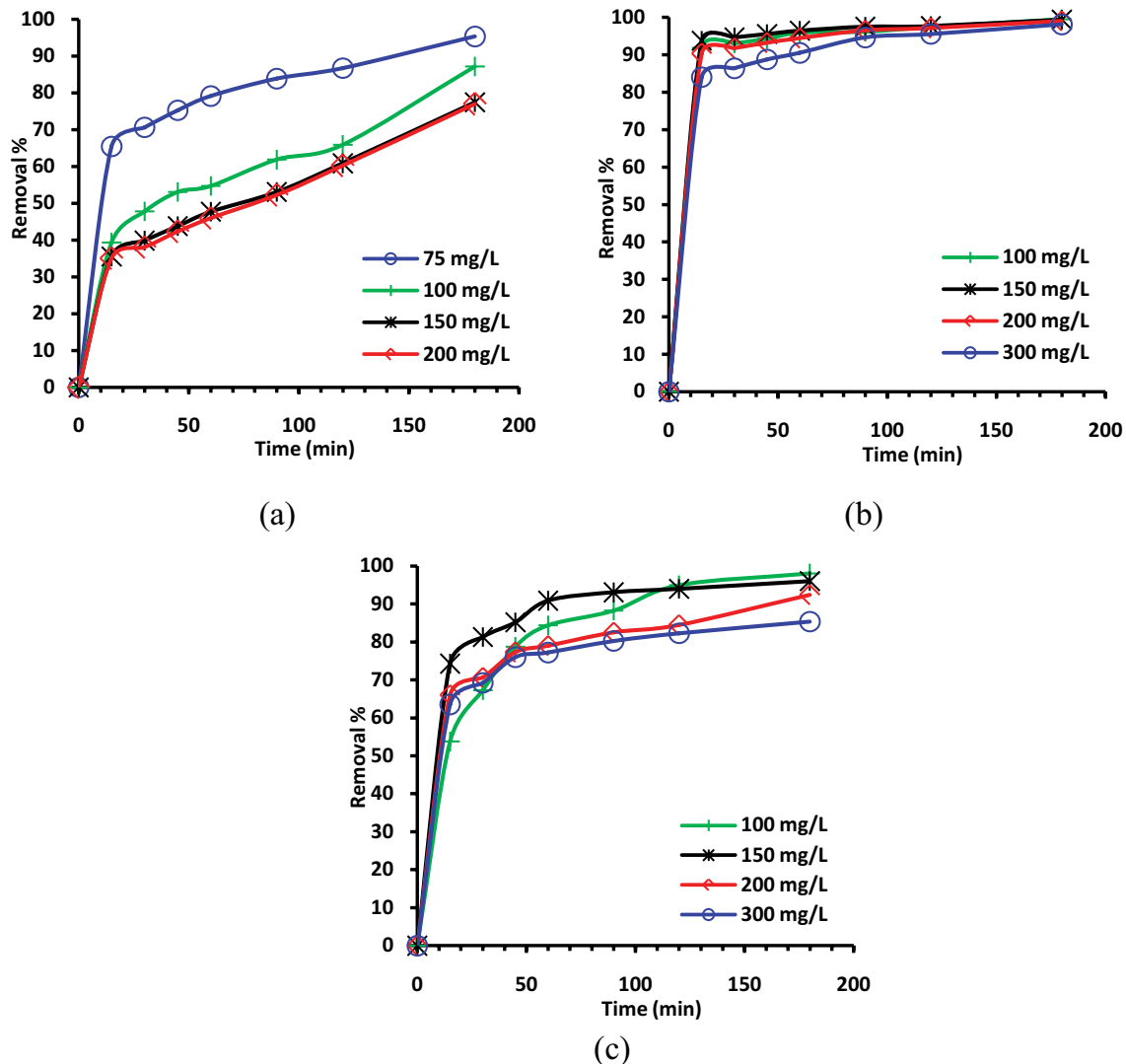


Fig. 5. Removal of AY11 dye (75–200 mg L<sup>-1</sup>) using (a) Melon-B (2.0 g L<sup>-1</sup>), removal of AY11 dye (100–300 mg L<sup>-1</sup>) using (b) Melon-BO-NH<sub>2</sub> (2.0 g L<sup>-1</sup>), and (c) Melon-BO-TETA (2.0 g L<sup>-1</sup>) at pH 1.0 and room temperature (25°C ± 2°C).

concentration of 150 mg L<sup>-1</sup> was 75% within 15 min, after 60 min the removal was 92% and did not change with an increase in time. The removal of dye was 65% within the first 15 min and after 60 min the removal became 75% then the removal increased slowly to reach the maximum value of about 81% for initial dye concentration 200 and 300 mg L<sup>-1</sup>.

From Fig. 5 the results showed that the contact time required to achieve equilibrium was about 3 h and there was rapid adsorption that occurred at initial contact time (15 min) by using the three different biochars. As mentioned before the most notable difference between the three biochars was the significantly higher removal of AY11 dye using the Melon-BO-NH<sub>2</sub> and Melon-BO-TETA modified biochars. The surface area and pore size distribution of the Melon-BO-NH<sub>2</sub> and Melon-BO-TETA modified biochars were slightly decreased after the modification process than would be expected based on BET analysis, while the surface charge enhanced probably due to the formation of amine sites on the surface of biochar. Amine sites produced a great chemical affinity between the AY11 dye and the biochar but the slow rate of dye adsorption after the first 15 min probably attributed to the slow pore diffusion of the solute ions into the bulk of adsorbent.

### 3.3.3. Effect of initial concentration on the removal of AY11 dye

The influence of the initial dye concentration on removal percentage and  $q_e$  was studied. The experiment was carried out at adsorbent doses using Melon-B biochar (2.0, 3.0, 4.0, 5.0 and 6.0 g L<sup>-1</sup>), pH 1.0 using a different initial concentration of AY11 dye (75–200 mg L<sup>-1</sup>) for 3 h at room temperature (25°C ± 2°C) (Fig. 6). The percentage of removal of AY11 dye decreased from 96% to 77% with an increase in the initial dye concentration from 75 to 200 mg L<sup>-1</sup> using Melon-B dose of biochar (2.0 g L<sup>-1</sup>) (Fig. 6a). The removal percentage of AY11 dye decreased from 97% to 85% with an increase in the initial dye concentration from 75 to 100 mg L<sup>-1</sup> and then increased again to 93% with an increase in the initial dye concentration from 100 to 200 mg L<sup>-1</sup> using Melon-B dose of biochar (3.0 g L<sup>-1</sup>). While the percentage of removal of AY11 dye decreases as the initial concentration of dye increased using Melon-B dose of biochar (4.0 g L<sup>-1</sup>). The percentage of removal of AY11 dye increased from 97% to 100% as the initial concentration of dye increased from 75 to 100 mg L<sup>-1</sup> and after that decreased with initial dye concentration increasing using Melon-B doses of biochar (5.0 and 6.0 g L<sup>-1</sup>) for an adsorbent dose of Melon-B biochar. Fig. 6b shows that the  $q_e$  decreases with an increase of Melon-B doses at the same initial concentration of AY11 dye, while it increases with the increase of initial dye concentration for all studied doses of Melon-B biochar. From Fig. 6b, the results indicate that the sorption capacities at equilibrium ( $q_e$ ) increased from 35.74 to 76.94, 24.26 to 61.92, 18.39 to 47.08, 14.72 to 38.95 and 12.27 to 32.50 mg g<sup>-1</sup> with an increase in the initial dye concentration from 75 to 100 to 150, and to 200 mg L<sup>-1</sup> using Melon-B doses 2.0, 3.0, 4.0, 5.0, and 6.0 g L<sup>-1</sup>, respectively.

The adsorption experiments at initial AY11 dye concentration from 100 to 300 mg L<sup>-1</sup> on its removal % using different Melon-BO-NH<sub>2</sub> doses (0.5, 1.0, 1.25, 1.50, and 2.0 g L<sup>-1</sup>) were also performed for 3 h at 25°C ± 2°C and the results are

represented in Fig. 6c. It is observed that the percentage of removal increased with increasing mass concentration of adsorbent from 0.5 to 2.0 g L<sup>-1</sup> and decreased with the increase of the initial dye concentrations from 100 to 300 mg L<sup>-1</sup>. The percentage of removal decreased from 94 to 67% with an increase in the initial concentration of AY11 dye from 100 to 300 mg L<sup>-1</sup> using 0.5 g L<sup>-1</sup> of Melon-BO-NH<sub>2</sub> biochar. The percentage of removal of dye decreased from 98.5% to 94% for an increase in the initial concentration of AY11 dye from 100 to 300 mg L<sup>-1</sup> using adsorbent dose 1.0 g L<sup>-1</sup> of Melon-BO-NH<sub>2</sub> biochar. Also, the removal percentage of dye decreased from 99% to 97% for an increase in dye initial concentration from 100 to 300 mg L<sup>-1</sup> using adsorbent dose 1.25 g L<sup>-1</sup> of Melon-BO-NH<sub>2</sub> biochar. The percentage of removal of dye decreased from 99.5% to 98% and from 100% to 99% for an increase in the initial concentration of AY11 dye from 100 to 300 mg L<sup>-1</sup> using adsorbent doses 1.50 and 2.0 g L<sup>-1</sup> of Melon-BO-NH<sub>2</sub> biochar, respectively.

The adsorption experiments at initial AY11 dye concentration ranged from 100 to 300 mg L<sup>-1</sup> on its removal percent of dye using different Melon-BO-TETA doses (0.5, 1.0, 1.25, 1.50, and 2.0 g L<sup>-1</sup>) were also performed for 3 h at 25°C ± 2°C and pH 1 (Fig. 6e). The removal percentage of AY11 dye using Melon-BO-TETA was increased with increasing of mass concentration of adsorbent from 0.5 to 2.0 g L<sup>-1</sup> and decreased with increasing of all initial dye concentrations. However, during using 1.50 g L<sup>-1</sup> adsorbent dose of Melon-BO-TETA biochar, the percentage of removal slightly decreased from 96% to 95% and then there was a slightly increased to 97%, after that there was another decreased to 90% with increasing of dye initial concentration from 100 to 300 mg L<sup>-1</sup>. The removal percent decreased when initial AY11 dye concentration increased for all the three different adsorbent biochars, which may be attributed to the saturation of adsorption sites on the biochar surface. The results represented in Fig. 6 show the  $q_e$  decreases with an increase of the Melon-BO-NH<sub>2</sub> and Melon-BO-TETA doses at the same initial concentration of AY11 dye, while it increases with an increase of initial dye concentration for all studied doses of Melon-BO-NH<sub>2</sub> and Melon-BO-TETA biochars.

The  $q_e$  onto the three different biochars at a lower initial concentration of AY11 dye were smaller than the corresponding adsorption capacities at equilibrium ( $q_e$ ) when higher initial concentrations were used. The decrease in  $q_e$  value was probably due to the concentration gradient between the adsorption vacant sites of the solid adsorbent and the concentration of dye solutions gets decreased with increasing adsorbent mass leading to decrease in  $q_e$  value or during the sorption process, there was an aggregation took place to lead to a reduction in surface area of the sorbent. The increase in the sorption capacities at equilibrium ( $q_e$ ) although using small doses of Melon-BO-NH<sub>2</sub> and Melon-BO-TETA (0.5 g L<sup>-1</sup>) and at a high initial concentration of dye was significant. The  $q_e$  increased to about seven times by using the modified biochars Melon-BO-NH<sub>2</sub> and Melon-BO-TETA than unmodified Melon-B biochar. This notable result may be attributed to the formation of amino reactive functional groups on the surface of biochars during the modification process that efficiently increased the negative surface charges and probably caused an increase in the sorption capacities at equilibrium ( $q_e$ ).

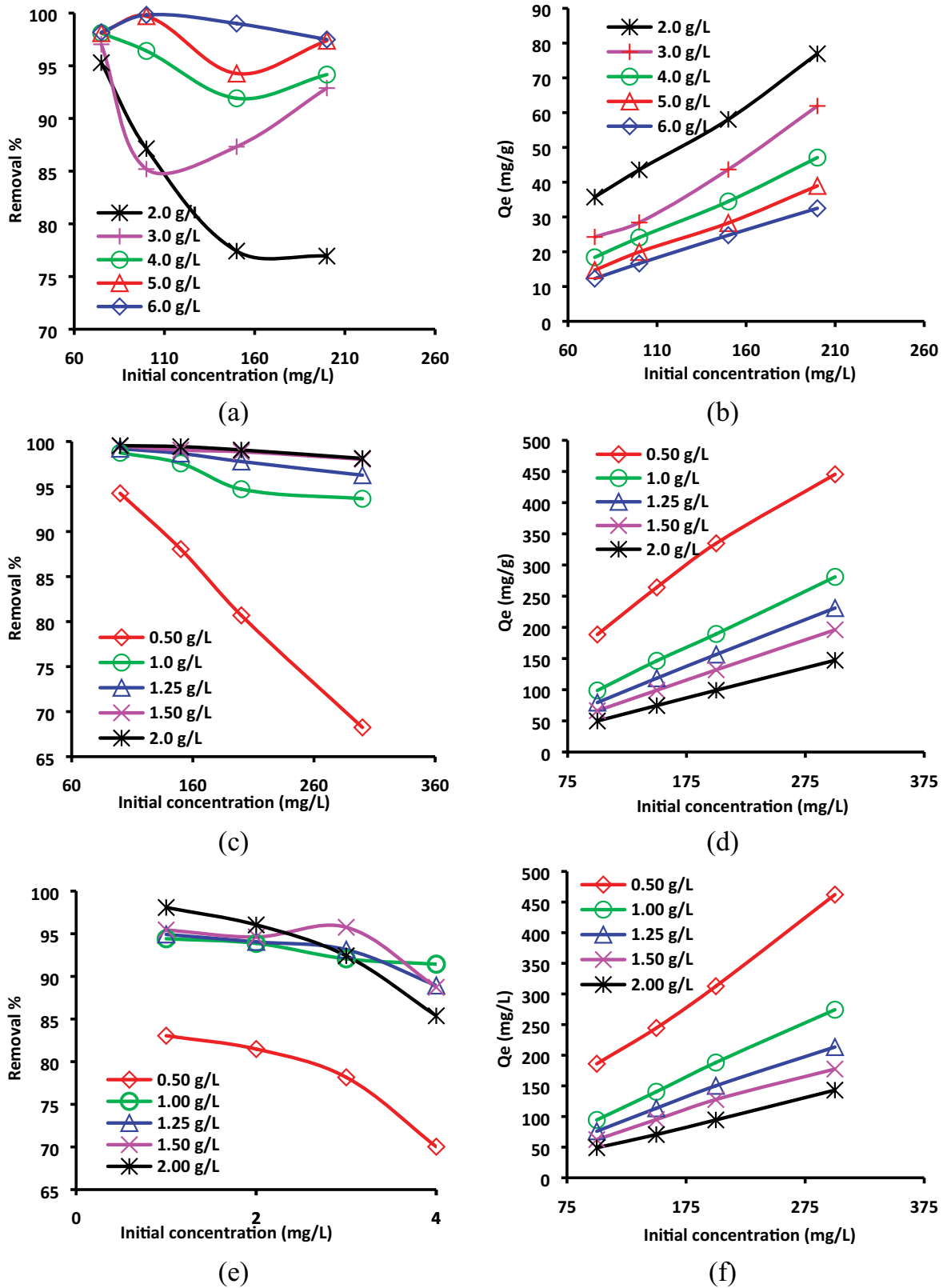


Fig. 6. Effect of AY11 initial concentration (75–200 mg L<sup>-1</sup>) on (a) removal %, (b)  $q_e$  (mg g<sup>-1</sup>) using different Melon-B doses (2.0–6.0 g L<sup>-1</sup>); effect of AY11 dye initial concentration (100–300 mg L<sup>-1</sup>) on (c) removal %, (d)  $q_e$  (mg g<sup>-1</sup>) using different Melon-BO-NH<sub>2</sub> doses (0.5–2.0 g L<sup>-1</sup>); effect of AY11 dye initial concentration (100–300 mg L<sup>-1</sup>) on (e) removal %, and (f)  $q_e$  (mg g<sup>-1</sup>) using different Melon-BO-TETA doses (0.5–2.0 g L<sup>-1</sup>) at room temperature (25°C ± 2°C).

### 3.3.4. Effect of adsorbent dosage on removal of AY11 dye

The effects of Melon-B dosage and the removal percentage of AY11 dye were studied by changing the adsorbent dose (2.0–6.0 g L<sup>-1</sup>) and the initial dye concentration (75–200 mg L<sup>-1</sup>), at room temperature (25°C ± 2°C) and pH 1 (Fig. 7). Fig. 7a indicates that the percentage of removal of AY11 dye was increased with increasing of the adsorbent doses (2.0–0.6 g L<sup>-1</sup>) for all initial concentrations of dye. The maximum removal percentage 100% was achieved using 6.0 g L<sup>-1</sup> of an adsorbent dose of Melon-B biochar at 100 g L<sup>-1</sup> initial dye concentration. Fig. 7b shows that the  $q_e$  decreases with an increase of Melon-B doses at the same initial concentration of AY11 dye, while it increases with the increase of initial dye concentration for all studied doses of Melon-B biochar. The results indicate that the  $q_e$  decreased from 35.74 to 12.27, 43.57 to 16.64, 58.06 to 24.75 and 76.94 to 32.50 mg g<sup>-1</sup> with an increase of Melon-B doses from 2.0 to 6.0 g L<sup>-1</sup> at initial dye concentrations (75, 100, 150, and 200 mg L<sup>-1</sup>), respectively. The influence of Melon-BO-NH<sub>2</sub> dosage on the removal percentage of AY11 dye was investigated in Fig. 7 by changing the quantity of adsorbent (0.5, 1.0, 1.25, 1.50, and 2.0 g L<sup>-1</sup>) and initial concentrations of AY11 dye (100, 150, 200, and 300 mg L<sup>-1</sup>) at pH 1 and room temperature (25°C ± 2°C) for 3 h. Fig. 7c indicates that the percentage of removal of AY11 dye was increased with increasing of the adsorbent doses (0.5–2.0 g L<sup>-1</sup>) for all initial concentrations of dye. The maximum removal percentage 99% was achieved using 2.0 g L<sup>-1</sup> of an adsorbent dose of Melon-BO-NH<sub>2</sub> biochar at 100 g L<sup>-1</sup> initial dye concentration. The effect of Melon-BO-TETA different doses (0.5, 1.0, 1.25, 1.5, and 2.0 g L<sup>-1</sup>) on removal % of different initial concentration (100, 150, 200, and 300 mg L<sup>-1</sup>) of AY11 dye at 25°C ± 2°C for 3 h was studied and reported in Fig. 7e. Fig. 7e indicates that the removal percentage of AY11 dye was increased with increasing of the adsorbent doses (0.5–2.0 g L<sup>-1</sup>) for all initial concentrations of dye. The maximum percentage of removal 97% was achieved using 2.0 g L<sup>-1</sup> of an adsorbent dose of Melon-BO-TETA biochar at 100 mg L<sup>-1</sup> initial dye concentration. The influence of Melon-BO-NH<sub>2</sub> and Melon-BO-TETA doses on the adsorption capacities at equilibrium ( $q_e$ ) was investigated, the Melon-BO-NH<sub>2</sub> and Melon-BO-TETA masses were varied between 0.5 and 2.0 g L<sup>-1</sup>, while initial dye concentration was varied between 100 and 300 mg L<sup>-1</sup>. The results are represented in Fig. 7d and f which show that the  $q_e$  decreases with increases of the Melon-BO-NH<sub>2</sub> and Melon-BO-TETA doses at the same initial concentration AY11 dye, while it increases with increases of initial dye concentration for all studied doses of Melon-BO-NH<sub>2</sub> and Melon-BO-TETA biochars. The results indicate that the  $q_e$  decreased from 188.50 to 49.77, 284.13 to 74.57, 354.75 to 99.06, and 445.48 to 147.18 mg g<sup>-1</sup> with an increase in Melon-BO-NH<sub>2</sub> doses (0.5, 1.0, 1.25, 1.50, and 2.0 g L<sup>-1</sup>) at initial dye concentrations (100, 150, 200 and 300 mg L<sup>-1</sup>), respectively (Fig. 7d). From Fig. 7f, the results indicate that the  $q_e$  decreased from 183.09 to 70.04, 290.44 to 78.53, 352.66 to 94.41, and 462.18 to 133.07 mg g<sup>-1</sup> with an increase of Melon-BO-TETA doses (0.5, 1.0, 1.25, 1.50, and 2.0 g L<sup>-1</sup>) at initial dye concentrations (100, 150, 200, and 300 mg L<sup>-1</sup>), respectively. These results can be attributed to the increased availability of active adsorption sites for AY11 dye ion binding.

The higher removal of dye by Melon-BO-NH<sub>2</sub> and Melon-BO-TETA than Melon-B biochars were caused by the synergy of amino functionality. The percentage of removal of AY11 dye increased to about 99% with the increase in the adsorbent dose to 2.0 g L<sup>-1</sup>.

### 3.4. Adsorption isotherm study

The adsorption isotherm is the relationship between the mass of adsorbent ( $q_e$  mg g<sup>-1</sup>) and of adsorbate concentration at equilibrium time ( $C_e$  in mg L<sup>-1</sup>) which explains how the adsorbate molecules are distributed between the liquid and solid phases at the equilibrium state [48,49]. The adsorption isotherm is important for calculating the maximum amount of adsorbate taken up by adsorbent ( $Q_m$  in mg g<sup>-1</sup>). There are several isotherms which help for the said calculations; however, Langmuir (Eq. (5)) [50,51], Freundlich (Eq. (6)) [52,53] and Temkin (Eq. (7)) [54,55] isotherms are selected to rationalize the dye-biochar interactions observed in this study. Their linear forms of these 3 isotherm equations are expressed as:

$$\frac{C_e}{q_e} = \frac{1}{K_L Q_m} + \frac{1}{Q_m} \times C_e \quad (5)$$

$$\log q_e = \log K_f + \frac{1}{n} \log C_e \quad (6)$$

$$q_e = \beta \ln A + \beta \ln C_e \quad (7)$$

where  $K_L$  (L mg<sup>-1</sup>) and  $Q_m$  (mg g<sup>-1</sup>) represent Langmuir constant and the maximum adsorption capacity calculated by the Langmuir model, respectively.  $K_f$  ((mg g<sup>-1</sup>) (L mg<sup>-1</sup>)<sup>1/n</sup>) and  $1/n$  are Freundlich constants that describe the adsorption density and intensity, respectively.  $A$  and  $B$  are the Temkin constant.

#### 3.4.1. Langmuir isotherm

The maximum adsorption capacity ( $Q_m$ ) corresponding to complete monolayer coverage on the sorbent surface was estimated by the Langmuir isotherm model. Values of Langmuir constants, the saturated monolayer sorption capacity ( $Q_m$ ), and the equilibrium adsorption constant,  $K_L$ , are represented in (Table 2) for the sorption of AY11 dye onto Melon-B, Melon-BO-NH<sub>2</sub> and Melon-BO-TETA biochars. The  $Q_m$  (mg g<sup>-1</sup>) values obtained from the Langmuir model were from 38.31–83.33 for Melon-B, 178.57–526.32 for Melon-BO-NH<sub>2</sub>, and 126.58–370.37 mg g<sup>-1</sup> for Melon-BO-TETA biochars. The adsorption of AY11 dye can be described by the model of Langmuir according to the higher correlation coefficient ( $R^2$ ). From Table 2, the correlation coefficients for the linear form of the Langmuir model ( $R^2$ ) ≥ 0.930 for Melon-B, 0.997 for Melon-BO-NH<sub>2</sub>, and 0.999 for Melon-BO-TETA biochars. It could be easily found that the Langmuir isotherm successfully explains the adsorption process as a monolayer formation of AY11 dye on the surface of Melon-BO-NH<sub>2</sub> and Melon-BO-TETA biochar.

Fig. 8 represented a relationship between  $C_e/q_e$  and  $C_e$  for Melon-B, Melon-BO-NH<sub>2</sub>, and Melon-TETA biochars.

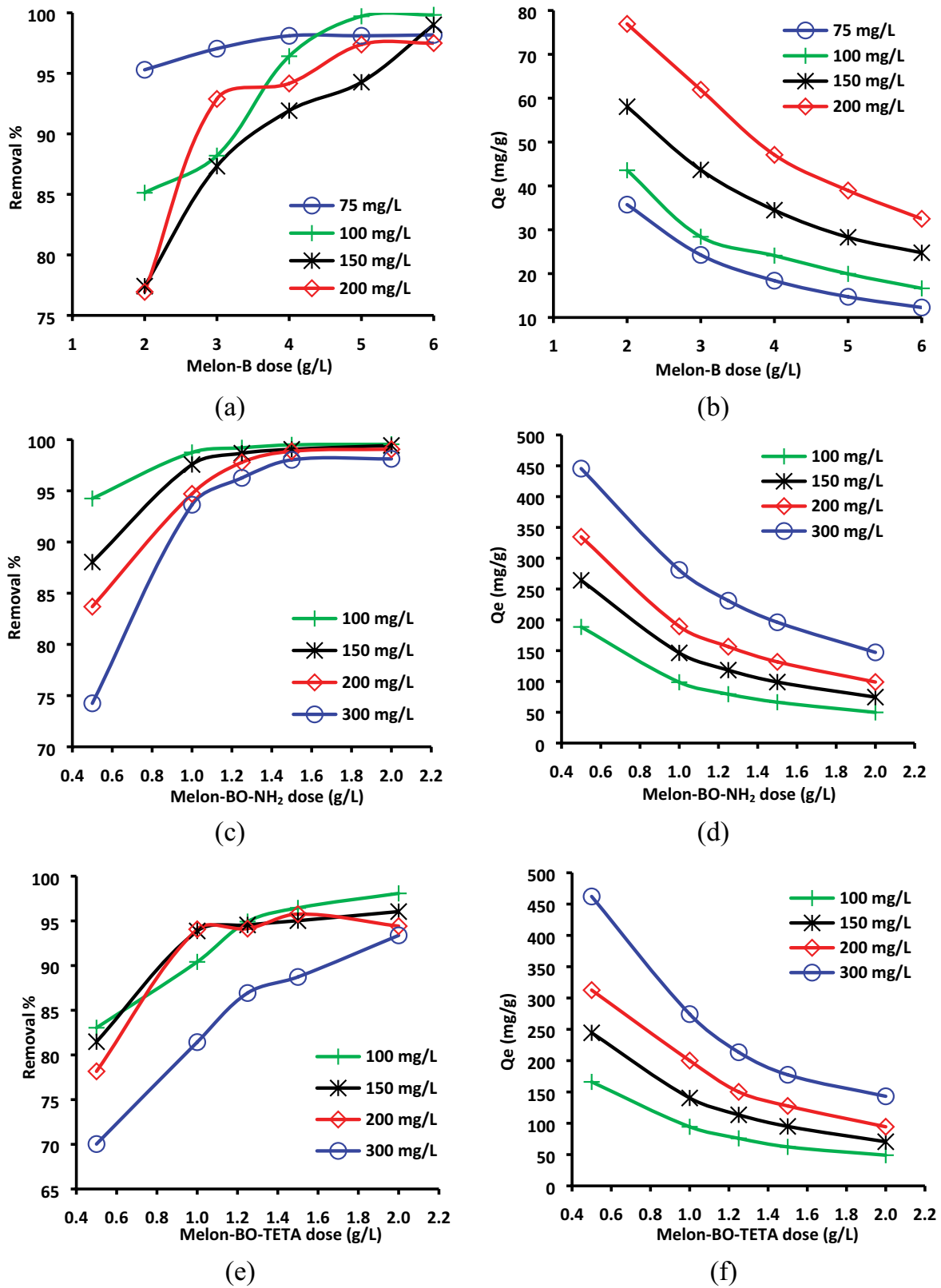


Fig. 7. Effect of Melon-B different doses (2.0–6.0 g L<sup>-1</sup>) on (a) removal %, (b)  $q_e$  (mg g<sup>-1</sup>) of different initial concentration (75–200 mg L<sup>-1</sup>); effect of Melon-BO-NH<sub>2</sub> different doses (0.5–2.0 g L<sup>-1</sup>) on (c) removal %, (d)  $q_e$  (mg g<sup>-1</sup>) of different initial concentration (100–300 mg L<sup>-1</sup>); effect of Melon-BO-TETA different doses (0.5–2.0 g L<sup>-1</sup>) on (e) removal %, and (f)  $q_e$  (mg g<sup>-1</sup>) of different initial concentration (100–300 mg L<sup>-1</sup>) of AY11 dye at 25°C ± 2°C.

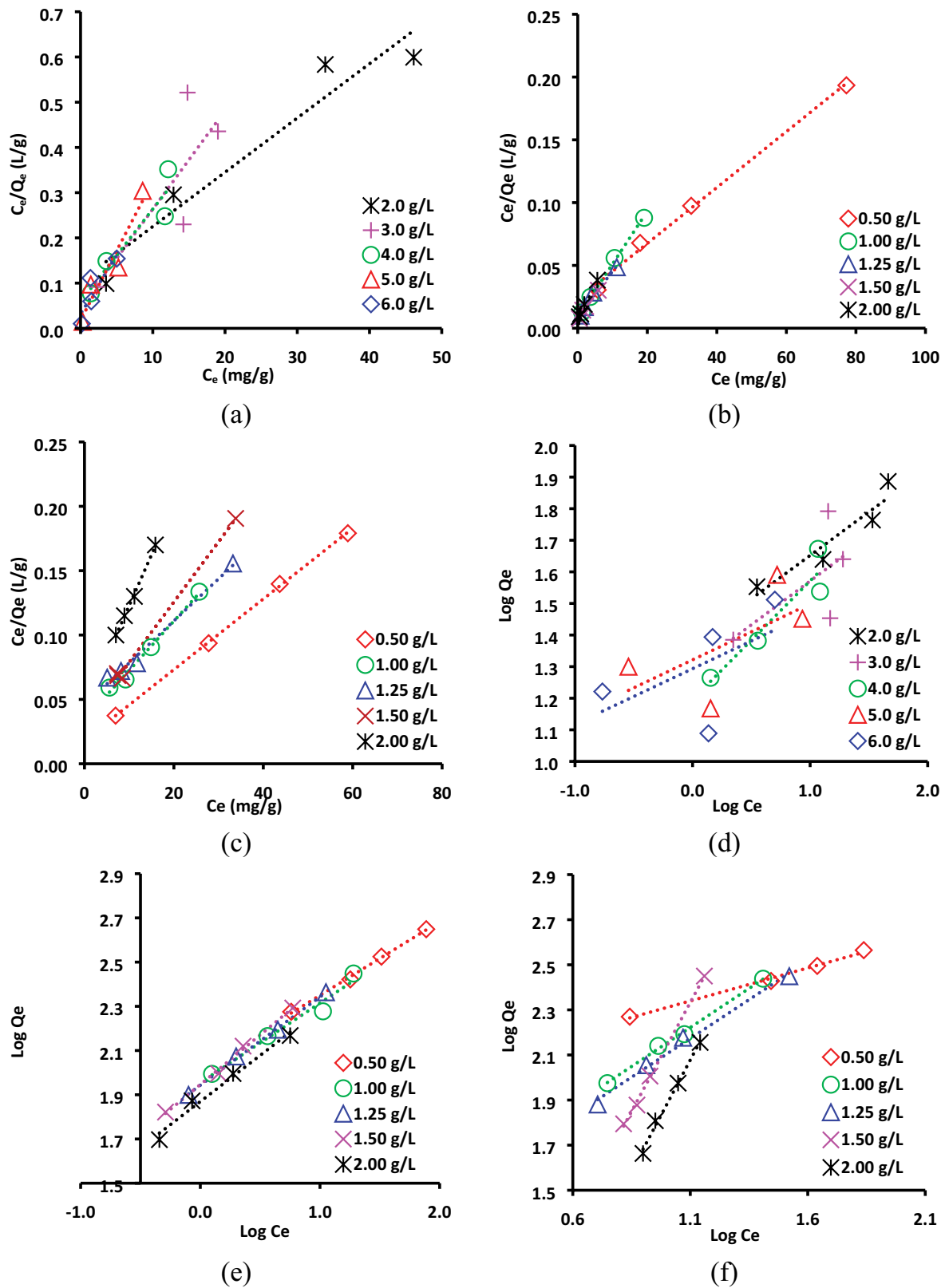


Fig. 8. Linearized Langmuir adsorption isotherm for AY11 dye of initial concentration (75–200 mg L<sup>-1</sup>) on (a) Melon-B doses (2.0–6.0 g L<sup>-1</sup>), of initial concentration (100–300 mg L<sup>-1</sup>) on (b) Melon-BO-NH<sub>2</sub>, (c) Melon-BO-TETA doses (0.5–2.0 g L<sup>-1</sup>), Freundlich adsorption isotherm for AY11 dye of initial concentration (75–200 mg L<sup>-1</sup>) on (d) Melon-B doses (2.0–6.0 g L<sup>-1</sup>), of initial concentration (100–300 mg L<sup>-1</sup>) on (e) Melon-BO-NH<sub>2</sub>, and (f) Melon-BO-TETA doses (0.5–2.0 g L<sup>-1</sup>) at 25°C ± 2°C.

The  $1/Q_m$ ,  $K_L$  and  $1/Q_m$  of the Langmuir model are, respectively, obtained from the intercept and the slope of the line. Tables S1–S3 represented the relation between  $q_e$  of AY11 at different initial concentrations obtained by batch experimental and  $q_e$  calculated using data from different isotherm models using different doses of Melon-B, Melon-BO-NH<sub>2</sub>, and Melon-TETA biochars, respectively, at room temperature ( $25^\circ\text{C} \pm 2^\circ\text{C}$ ). There was an agreement between the  $q_e$  obtained from batch experimental and  $q_e$  calculated using data from the Langmuir isotherm model which proves the applicability of the Langmuir model [56,57].

### 3.4.2. Freundlich isotherm

Though Freundlich isotherm correctly established the adsorption process as a heterogeneous phenomenon, the linear fitting parameters from the model of Freundlich isotherm for the removal of AY11 dye by Melon-B, Melon-BO-NH<sub>2</sub>, and Melon-BO-TETA biochars are listed in Table 2. Fig. 8 represents the plot of  $\log(q_e)$  vs.  $\log(C_e)$  with the intercept value of  $\log K_F$  and the slope of  $1/n_F$ . In the Freundlich model, when  $1/n$  is less than 1, it is relatively easy for adsorbent to adsorb solute and the adsorption of dye on the adsorbent is a favorable physical process. Since

Table 2

Isotherm study data of adsorption of AY11 dye of different initial concentration onto Melon-B, Melon-BO-NH<sub>2</sub>, and Melon-BO-TETA of different adsorbent doses at  $25^\circ\text{C} \pm 2^\circ\text{C}$

Isotherm model	Isotherm parameter	Melon-B doses ( $\text{g L}^{-1}$ )				
		2.0	3.0	4.0	5.0	6.0
Langmuir	$Q_m$ ( $\text{mg g}^{-1}$ )	83.33	45.87	48.78	32.47	38.31
	$K_L$	0.11	0.48	0.35	1.73	0.83
	$R^2$	0.930	0.651	0.886	0.914	0.762
	$1/n$	0.275	0.278	0.375	0.177	0.176
Freundlich	$K_F$ ( $\text{mg}^{1-1/n} \text{L}^{1/n} \text{g}^{-1}$ )	23.82	19.66	15.70	20.97	19.65
	$Q_m$ ( $\text{mg g}^{-1}$ )	72.58	60.49	72.15	47.41	44.14
	$R^2$	0.901	0.421	0.888	0.409	0.329
	$A_T$	2.62	5.64	3.29	134.50	148.96
Temkin	$B_T$	14.26	9.88	10.93	4.53	4.19
	$R^2$	0.829	0.329	0.798	0.425	0.430
		Melon-BO-NH <sub>2</sub> dose ( $\text{g L}^{-1}$ )				
		0.50	1.00	1.25	1.50	2.00
Langmuir	$Q_m$ ( $\text{mg g}^{-1}$ )	526.32	322.58	277.78	256.41	178.57
	$K_L$	0.07	0.231	0.38	0.53	0.79
	$R^2$	0.996	0.997	0.982	0.978	0.996
	$1/n$	0.334	0.360	0.399	0.449	0.418
Freundlich	$K_F$ ( $\text{mg}^{1-1/n} \text{L}^{1/n} \text{g}^{-1}$ )	103.78	90.05	87.74	88.35	73.99
	$Q_m$ ( $\text{mg g}^{-1}$ )	401.55	388.79	444.85	696.95	506.29
	$R^2$	0.997	0.970	0.998	0.995	0.981
	$A_T$	1.086	3.758	4.427	4.063	7.936
Temkin	$B_T$	99.444	59.512	58.635	59.960	38.205
	$R^2$	0.995	0.988	0.991	0.990	0.995
		Melon-BO-TETA dose ( $\text{g L}^{-1}$ )				
		0.50	1.00	1.25	1.50	2.00
Langmuir	$Q_m$ ( $\text{mg g}^{-1}$ )	370.37	263.16	303.03	212.77	126.58
	$K_L$	0.15	0.11	0.07	0.15	0.18
	$R^2$	1.000	0.999	0.989	0.996	0.998
	$1/n$	0.29	0.69	0.69	1.97	1.93
Freundlich	$K_F$ ( $\text{mg}^{1-1/n} \text{L}^{1/n} \text{g}^{-1}$ )	104.28	28.87	26.10	0.81	1.61
	$Q_m$ ( $\text{mg g}^{-1}$ )	340.86	493.61	437.76	7,097.41	11,838.59
	$R^2$	0.9945	0.997	0.992	0.993	0.999
	$A_T$	0.63	0.34	0.59	0.67	0.17
Temkin	$B_T$	105.47	116.71	73.04	58.33	165.40
	$R^2$	0.771	0.851	0.989	0.822	0.978

the values of  $1/n$  are smaller than one, then the adsorption of acid AY11 dye is considered more favorable on Melon-B as well as Melon-BO-NH<sub>2</sub> than the Melon-BO-TETA biochars. Further, it is obvious the values of the correlation coefficient for Figs. 8d–f suggests that Freundlich isotherm successfully explains the variation of  $\log q_e$  as a function of  $\log C_e$ . Table 2 showed Freundlich  $Q_m$  equal 72.58 for Melon-B, 696.95 for Melon-BO-NH<sub>2</sub>, and 493.61 mg g<sup>-1</sup> for Melon-BO-TETA biochars. The higher the  $Q_m$  value, the better the adsorption of AY11 dye. Tables S1–S3 represented the relation between  $q_e$  of AY11 dye obtained from experiments and  $q_e$  obtained from Freundlich isotherm model analysis on the various doses of Melon-B, Melon-BO-NH<sub>2</sub>, and Melon-BO-TETA, respectively. A reliable value of calculated  $q_e$  was founded in accordance with that obtained from the Freundlich isotherm model for all data collection.

### 3.4.3. Temkin isotherm

Temkin isotherm takes into account the heat changes associated with the adsorption process due to indirect adsorbent/adsorbate interactions; it is also assumed that the heat of adsorption of all molecules in the layer decreases linearly as a result of increase surface coverage. Temkin isotherm parameters of the adsorption of AY11 dye by Melon-B, Melon-BO-NH<sub>2</sub>, and Melon-BO-TETA biochars were obtained from Fig. 9. The Temkin constants were estimated and listed in Table 2. The value of the heat of adsorption indicating a physical adsorption process occurred. The correlation coefficients values obtained from Temkin isotherm  $R^2 > 0.83$  for Melon-B, 0.995 for Melon-BO-NH<sub>2</sub> and 0.989 for Melon-BO-TETA biochars indicated that Temkin model can be successfully applied to study the heat changes associated with adsorption of AY11 dye by Melon-BO-NH<sub>2</sub> and Melon-BO-TETA. Tables S1–S3 show the values of experimental and calculated amounts of dye adsorbed at equilibrium  $q_e$  by using Temkin model. The results are more applicable with Melon-BO-NH<sub>2</sub> biochar in all different adsorbent doses or initial dye concentrations but they were only applicable when used a high adsorbent dose for the two other biochars.

### 3.5. Error function studies for best-fit isotherm model

Several different error functions such as the average percentage errors [58], Chi-square error ( $\chi^2$ ) [59], the root mean square errors [58], the hybrid fractional error function [59,60], the sum of the absolute errors [58], Marquardt's percent standard deviation [58] was used to find the best-fit isotherm model for the experimental data and to detect the error distribution between the experimental equilibrium data and predicted isotherms.

$$APE(\%) = \frac{100}{N} \times \sum_{i=1}^N \left| \frac{q_{e, \text{isotherm}} - q_{e, \text{calc.}}}{q_{e, \text{isotherm}}} \right|_i \quad (8)$$

$$HYBRID = \frac{100}{N-P} \times \sum_{i=1}^N \left| \frac{q_{e, \text{isotherm}} - q_{e, \text{calc.}}}{q_{e, \text{isotherm}}} \right|_i \quad (9)$$

$$\chi^2 = \sum_{i=1}^N \frac{(q_{e, \text{isotherm}} - q_{e, \text{calc.}})^2}{q_{e, \text{isotherm}}} \quad (10)$$

$$MPSD = 100 \times \sqrt{\frac{1}{N-P} \sum_{i=1}^N \frac{(q_{e, \text{calc.}} - q_{e, \text{isotherm}})^2}{q_{e, \text{isotherm}}}} \quad (11)$$

$$EABS = \sum_{i=1}^N |q_{e, \text{calc.}} - q_{e, \text{isotherm}}|_i \quad (12)$$

$$RMS = 100 \times \sqrt{\frac{1}{N} \sum_{i=1}^N \left( 1 - \frac{q_{e, \text{calc.}}}{q_{e, \text{isotherm}}} \right)^2} \quad (13)$$

The calculated isotherm parameters by six error functions between experimental data and theoretical isotherms are given in Table 3 for Melon-B, Melon-BO-NH<sub>2</sub>, and Melon-BO-TETA biochars, respectively. From Table 3, it can be observed that the Freundlich isotherm model is comparable and applicable to the experimental equilibrium data for Melon-B and Melon-BO-NH<sub>2</sub> biochars. The Langmuir model is the best-fit isotherm model to the experimental data for Melon-BO-TETA biochar.

### 3.6. Adsorption kinetic studies

The solute uptake rate process of AY11 dye onto Melon-B, Melon-BO-NH<sub>2</sub> and Melon-BO-TETA biochars is required for selecting optimum operating conditions for the full-scale batch process and have been investigated by applying pseudo-first-order [61], pseudo-second-order [62], Elovich [63–65] and intraparticle diffusion [66,67] equations. The conformity between experimental data and model predicted values was expressed by the correlation coefficients ( $R^2$ ).

#### 3.6.1. Pseudo-first-order kinetic model

Parameters for the pseudo-first-order kinetics (Eq. (14)) of AY11 dye adsorption by Melon-B, Melon-BO-NH<sub>2</sub> and Melon-BO-TETA biochars are represented by the graphical representation of values of  $\log(q_e - q_t)$  against  $t$  in Fig. 10. The values of  $k_1$  (rate constant) and the  $q_e$  can be measured from the slope and intercept of the plot, respectively. The  $R^2$  values show that the pseudo-first-order model did not explain the adsorption mechanism to a satisfactory level. It is also obvious that  $q_e$  values calculated theoretically are, however, in far relation with the  $q_e$  values calculated experimentally (Tables 4–6).

$$\log(q_e - q_t) = \log(q_e) - \frac{k_1}{2.303} t \quad (14)$$

#### 3.6.2. Pseudo-second-order kinetic model

The pseudo-second-order model of AY11 dye by Melon-B, Melon-BO-NH<sub>2</sub>, and Melon-BO-TETA biochars was studied to investigate the promoting effect of amine groups on the

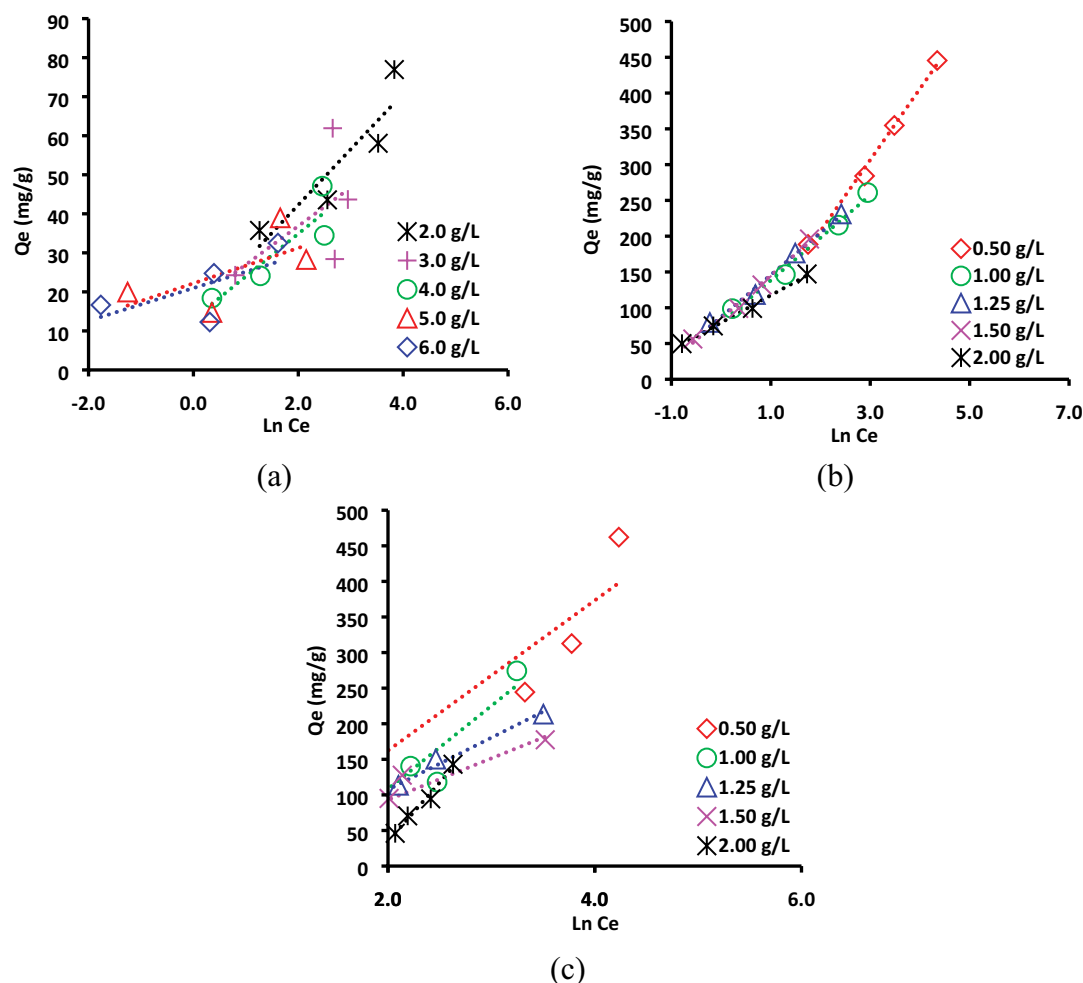


Fig. 9. Temkin adsorption isotherm for AY11 dye of initial concentration (75–200 mg L<sup>-1</sup>) on (a) Melon-B (2.0–6.0 g L<sup>-1</sup>); of initial concentration (100–300 mg L<sup>-1</sup>) on (b) Melon-BO-NH<sub>2</sub> and (c) Melon-BO-TETA doses (0.5–2.0 g L<sup>-1</sup>) at 25°C ± 2°C.

Table 3

Best-fit isotherm model to the experimental equilibrium data by several different errors functions for AY11 dye onto Melon-B, Melon-BO-NH<sub>2</sub> and Melon-BO-TETA at 25°C ± 2°C

Isotherm model	APE %	χ <sup>2</sup>	HYBRID	MPSD	EABS	RMS
Melon-B						
Linear-Langmuir	0.25	0.25	2.40	0.11	5.43	0.11
Freundlich	0.19	0.19	1.64	0.07	5.74	0.07
Temkin	0.22	0.22	1.90	0.09	4.56	0.09
Melon-BO-NH <sub>2</sub>						
Linear-Langmuir	0.07	0.07	1.33	0.01	6.02	0.01
Freundlich	0.03	0.03	0.17	0.00	4.17	0.00
Temkin	0.05	0.05	0.44	0.00	5.36	0.00
Melon-BO-TETA						
Linear-Langmuir	0.09	0.09	2.69	0.02	7.40	0.02
Freundlich	0.26	0.26	17.59	0.16	31.57	0.16
Temkin	0.12	0.12	3.59	0.03	18.60	0.03

APE – average percentage errors; χ<sup>2</sup> – Chi-square error; HYBRID – hybrid fractional error function; MPSD – Marquardt’s percent standard deviation; EABS – sum of the absolute errors; RMS – root mean square errors.

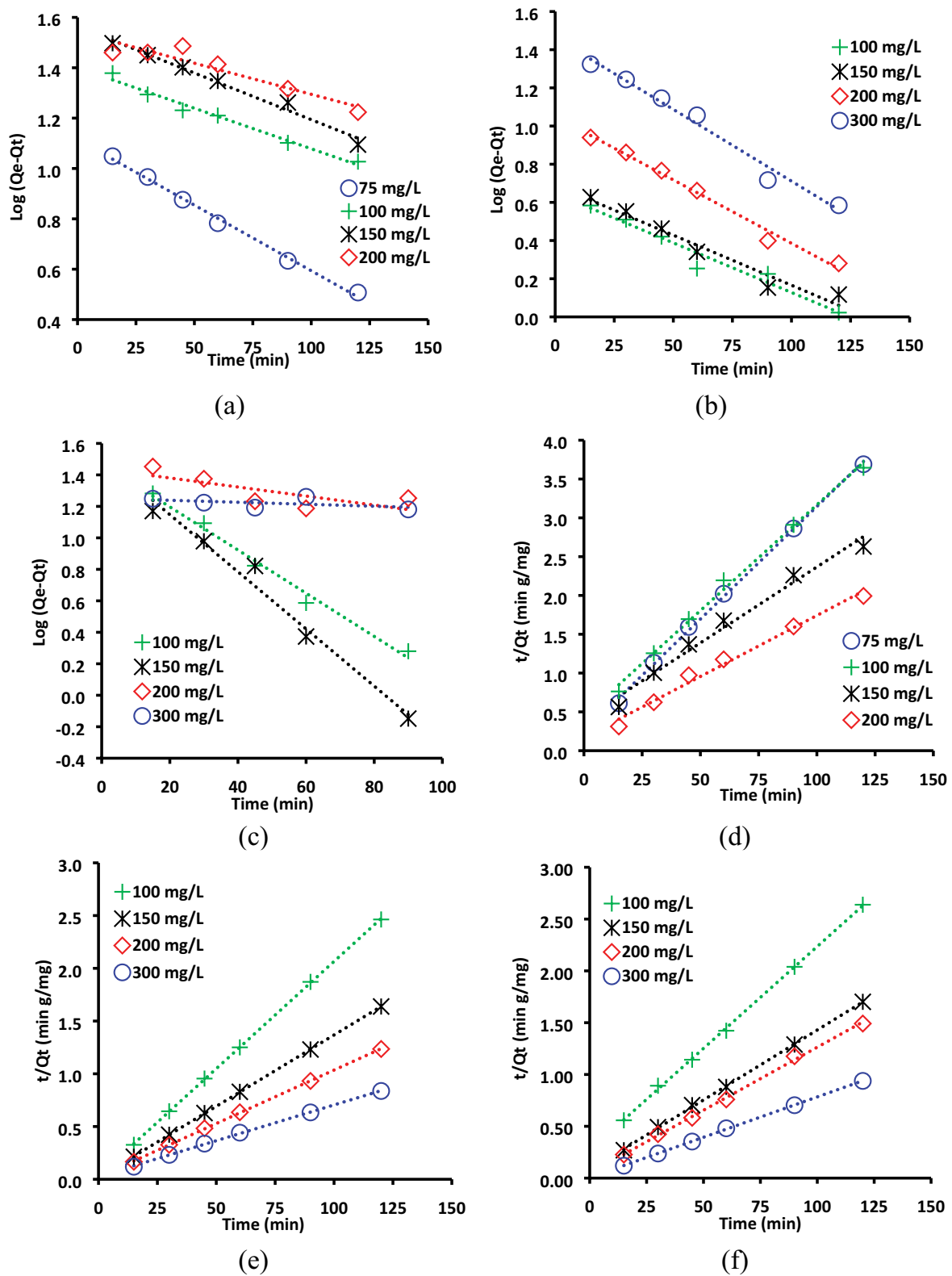


Fig. 10. Pseudo-first-order kinetic of adsorption of AY11 dye of initial concentration (75–200 mg L<sup>-1</sup>) by (a) Melon-B, of initial concentration (100–300 mg L<sup>-1</sup>) by (b) Melon-BO-NH<sub>2</sub> and (c) Melon-BO-TETA adsorbent dose (2.0 g L<sup>-1</sup>) at 25°C ± 2°C. Pseudo-second-order kinetic of adsorption of AY11 dye of initial concentration (75–200 mg L<sup>-1</sup>) by (d) Melon-B adsorbent dose (2.0 g L<sup>-1</sup>); of initial concentration (100–300 mg L<sup>-1</sup>) by (e) Melon-BO-NH<sub>2</sub> and (f) Melon-BO-TETA adsorbent dose (2.0 g L<sup>-1</sup>) at 25°C ± 2°C.

Table 4

Pseudo-first-order and pseudo-second-order results of adsorption of AY11 dye of different initial concentration (75, 100, 150, and 200 mg L<sup>-1</sup>) onto Melon-B of different adsorbent doses (2, 3, 4, 5, and 6 g L<sup>-1</sup> dye solution)

Parameter		Pseudo-first-order				Pseudo-second-order			
Melon-B doses (g L <sup>-1</sup> )	AY11 dye (mg L <sup>-1</sup> )	$q_{e,exp.}$	$q_{e,calc.}$	$k_1 \times 10^3$	$R^2$	$q_{e,calc.}$	$k_2 \times 10^3$	$H$	$R^2$
2.0	75	35.74	13.03	11.98	0.995	34.48	3.43	4,078	0.999
	100	43.57	25.14	7.37	0.980	39.63	1.69	2,266	0.995
	150	58.06	36.69	8.52	0.983	56.02	0.94	2,436	0.980
	200	76.94	34.82	5.76	0.886	73.69	1.45	5,896	0.986
3.0	75	24.26	9.06	15.66	0.961	24.33	4.68	2,768	1.000
	100	28.40	15.38	9.44	1.000	26.91	2.48	1,662	0.993
	150	43.66	25.46	11.05	0.995	41.49	1.33	2,284	0.995
	200	61.92	29.20	9.44	0.993	59.82	1.43	4,623	0.995
4.0	75	18.39	5.24	22.34	0.969	18.83	9.35	3,317	1.000
	100	24.10	12.09	13.13	0.997	23.64	3.06	1,709	0.995
	150	34.47	18.42	11.28	0.998	32.79	1.97	2,119	0.993
	200	47.08	23.06	10.13	0.993	43.67	1.74	3,317	0.996
5.0	75	14.72	3.83	22.80	0.952	15.04	13.05	2,951	1.000
	100	19.94	6.45	16.12	0.974	19.96	7.11	2,831	0.999
	150	28.28	15.34	13.59	0.998	28.09	2.25	1,773	0.995
	200	38.95	16.26	14.28	0.987	38.61	2.50	3,734	0.999
6.0	75	12.27	2.72	23.26	0.960	12.48	19.75	3,079	1.000
	100	16.64	5.02	16.12	0.941	16.58	9.51	2,616	0.999
	150	24.75	7.60	17.73	0.990	25.00	6.14	3,837	1.000
	200	32.50	11.48	16.12	0.724	32.79	3.45	3,713	0.996

Table 5

Pseudo-first-order and pseudo-second-order results of adsorption of AY11 dye of different initial concentration (100–300 mg L<sup>-1</sup>) onto Melon-BO-NH<sub>2</sub> of different adsorbent doses (0.5–2.0 g L<sup>-1</sup> dye solution) at 25°C

Parameter		Pseudo-first-order				Pseudo-second-order			
Melon-BO-NH <sub>2</sub> doses (g L <sup>-1</sup> )	AY11 dye (mg L <sup>-1</sup> )	$q_{e,exp.}$	$q_{e,calc.}$	$k_1 \times 10^3$	$R^2$	$q_{e,calc.}$	$k_2 \times 10^3$	$H$	$R^2$
0.50	100	188.50	122.24	10.82	0.954	181.82	0.23	7,663	0.993
	150	284.13	246.04	10.82	0.951	384.62	0.02	3,413	0.898
	200	354.75	355.71	10.59	0.946	256.41	0.02	1,246	0.225
	300	445.48	390.93	7.37	0.763	588.24	0.014	4,755	0.652
1.00	100	98.75	20.88	12.67	0.987	97.09	2.45	23,095	1.000
	150	146.36	50.75	15.66	0.972	147.06	0.85	18,282	0.998
	200	215.41	105.44	15.43	0.997	192.31	0.32	11,765	0.995
	300	260.93	240.05	14.05	0.990	333.33	0.06	6,725	0.986
1.25	100	79.36	7.593	12.90	0.945	78.74	7.47	46,296	1.000
	150	118.41	23.01	15.43	0.977	117.65	2.20	30,395	1.000
	200	156.45	55.26	15.43	0.998	156.25	0.78	19,157	0.998
	300	231.03	154.31	13.59	0.989	238.10	0.17	9,662	0.993
1.50	100	56.33	6.09	12.21	0.968	65.36	9.52	40,650	1.000
	150	99.05	6.11	12.67	0.952	98.04	9.72	93,458	1.000
	200	131.82	20.03	15.89	0.994	131.58	2.60	45,045	1.000
	300	196.05	120.28	4.61	0.990	200.00	0.59	23,419	0.998
2.00	100	49.77	4.44	11.98	0.957	49.26	13.04	31,646	1.000
	150	74.57	4.91	11.98	0.958	74.07	12.07	66,225	1.000
	200	99.06	11.22	15.20	0.988	99.01	4.77	46,729	1.000
	300	147.18	29.05	17.27	0.981	147.06	1.74	37,594	0.999

Table 6

Pseudo-first-order and pseudo-second-order results of adsorption of AY11 dye of different initial concentration (100–300 mg L<sup>-1</sup>) onto Melon-BO-TETA of different adsorbent doses (0.5–2.0 g L<sup>-1</sup> dye solution) at 25°C

Melon-BO-TETA Doses (g L <sup>-1</sup> )	Parameter AY11 dye (mg L <sup>-1</sup> )	Pseudo-first-order				Pseudo-second-order			
		$q_{e,exp.}$	$q_{e,calc.}$	$k_1 \times 10^3$	$R^2$	$q_{e,calc.}$	$k_2 \times 10^3$	$H$	$R^2$
0.50	100	183.09	138.58	7.83	0.969	163.93	0.19	5.0E+03	0.994
	150	290.44	108.44	6.22	0.952	204.08	0.53	2.2E+04	0.995
	200	352.66	158.05	12.14	0.955	250.00	0.36	2.3E+04	0.996
	300	462.18	184.97	1.38	0.988	452.50	1.15	1.1E+05	1.000
1.00	100	94.41	60.56	11.98	0.983	93.46	0.47	4.1E+03	0.997
	150	140.41	53.31	4.84	0.917	113.64	1.52	2.0E+04	0.998
	200	180.12	61.80	3.22	0.634	177.06	2.02	4.4E+04	0.996
	300	274.30	84.08	3.22	0.688	272.22	1.35	6.7E+04	0.998
1.25	100	75.94	38.63	12.44	0.941	74.07	0.93	5.1E+03	1.000
	150	113.46	35.40	5.76	0.981	108.04	1.96	1.9E+04	0.998
	200	140.17	53.94	4.15	0.861	140.48	1.82	2.6E+04	1.000
	300	213.43	38.49	-0.23	0.005	209.49	-4.58	-1.3E+05	0.998
1.50	100	88.30	47.48	27.87	0.991	69.93	0.76	3.7E+03	0.999
	150	95.02	31.67	7.83	0.997	96.21	1.73	1.3E+04	0.998
	200	127.68	43.87	11.05	0.999	121.95	1.06	1.6E+04	0.998
	300	177.45	30.73	-0.46	0.008	172.86	-8.31	-1.7E+05	0.996
2.00	100	70.04	31.25	32.93	0.994	70.76	1.45	3.7E+03	0.999
	150	78.53	20.30	29.71	0.873	74.07	2.31	1.3E+04	1.000
	200	94.41	26.43	5.76	0.678	91.97	3.19	2.1E+04	0.998
	300	133.07	17.77	1.38	0.431	128.21	12.94	2.1E+05	1.000

adsorption kinetics and was presented in Fig. 10. The values of adsorption rate constant  $k_2$  and equilibrium adsorption capacity  $q_e$  for pseudo-second-order adsorptions can be calculated from the intercept and slope of the plots of  $t/q_t$  vs.  $t$ .

$$\left(\frac{t}{q_t}\right) = \frac{1}{k_2 q_e^2} + \frac{1}{q_e} (t) \quad (15)$$

The data analysis shows that the correlation coefficients ( $R^2$ ) for fitting the data to the pseudo-second-order kinetic model are ranged to about 1.0. Additionally, in contrast to the values of  $q_e$  calculated using the pseudo-first-order, the theoretical values of  $q_e$  determined using the pseudo-second-order kinetic model agree very well with the experimental ones ( $Q_{exp.}$ ) (Tables 4–6). Both facts suggest that the pseudo-second-order mechanism is more applicable to the adsorption of AY11 dye by Melon-B, Melon-BO-NH<sub>2</sub>, and Melon-BO-TETA biochars, which relies to the assumption that physical adsorption, may be the rate-limiting step.

### 3.6.3. Elovich kinetic model

The Elovich equation describes a chemical adsorption mechanism in nature and it is the rate equation based on the adsorption capacity.

$$q_t = \frac{1}{\beta} \ln(\alpha\beta) + \frac{1}{\beta} \ln(t) \quad (16)$$

Fig. 11 depicts the plot of  $q_t$  vs.  $\ln(t)$ . The Elovich constants  $\alpha$  (initial adsorption rate) and  $\beta$  (desorption constant) were calculated from the intercept and slope of the straight line, are listed in Tables 7–9. From, Tables 7–9, it can observe that the correlation coefficients  $R^2$  are very high for Melon-B and Melon-BO-NH<sub>2</sub> adsorbents. Also, the correlation coefficients are high for Melon-BO-TETA biochar except with high initial dye concentration at high adsorbent dose, the correlation coefficients are very low. The values of  $R^2$  obtained in the present study indicate that chemical sorption processes may be the rate-limiting in the adsorption of AY11 dye onto Melon-B and Melon-BO-NH<sub>2</sub> biochars, while in the case of Melon-BO-TETA biochar the adsorption of dye seems to involve physisorption only at high initial dye concentration and high adsorbent dose.

### 3.6.4. Intraparticle diffusion model

Weber and Morris [66,67] thought that if they plot  $q_t$  and the square root values of time, a linear relation passes through the origin will be occurred when the adsorption is controlled by intraparticle diffusion step. However, if the line does not pass through the origin, a larger  $C$  indicates that the film diffusion will greatly affect the rate of the adsorption process. The effect of intraparticle diffusion resistance on adsorption can be determined using the following equation 17 [66,67].

$$q_t = K_{diff} t^{1/2} + C \quad (17)$$

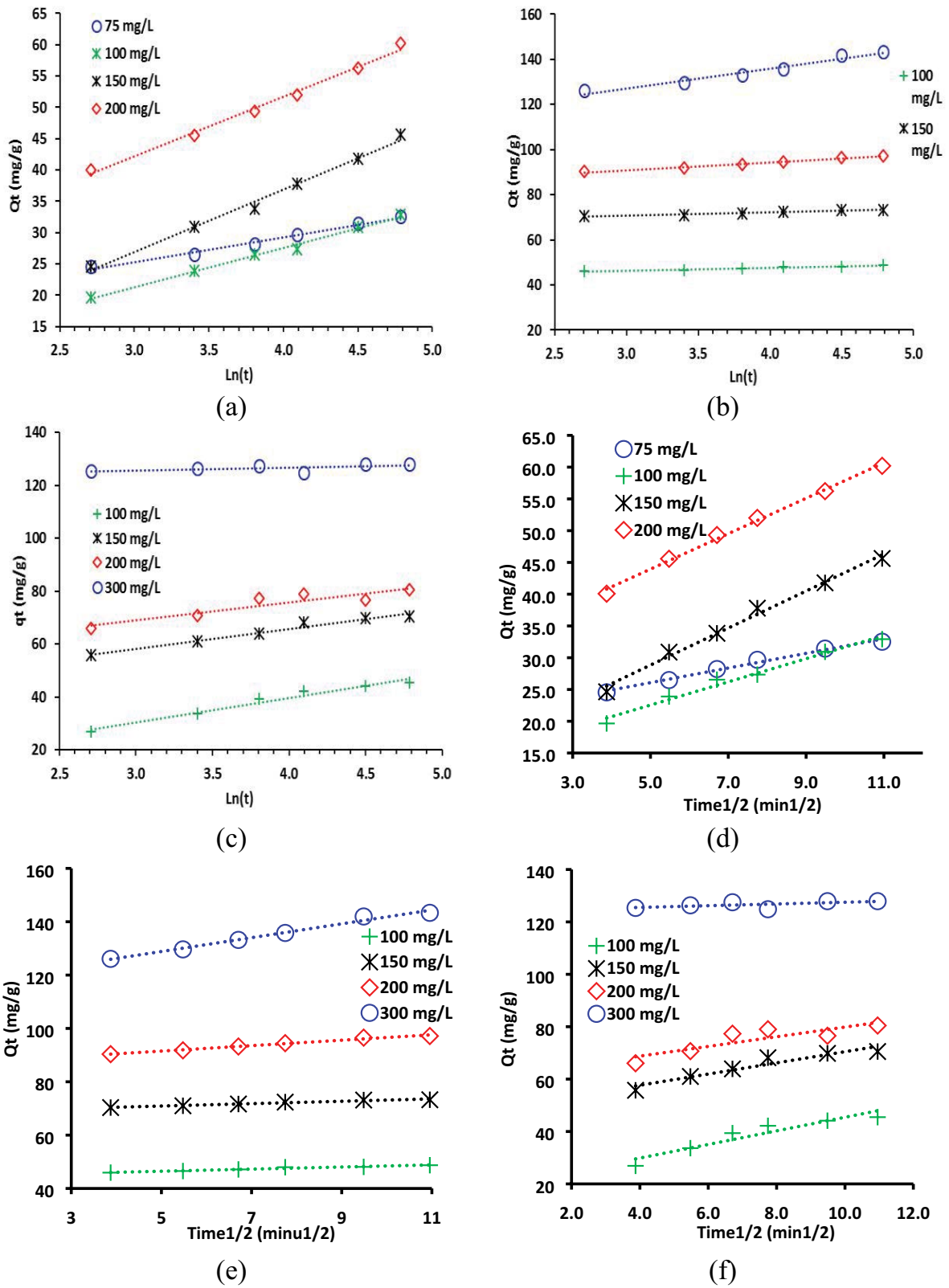


Fig. 11. Elovich kinetic of adsorption of AY11 dye of initial concentration (75–200 mg L<sup>-1</sup>) by (a) Melon-B adsorbent dose (2.0 g L<sup>-1</sup>); of initial concentration (100–300 mg L<sup>-1</sup>) by (b) Melon-BO-NH<sub>2</sub>, (c) Melon-BO-TETA adsorbent dose (2.0 g L<sup>-1</sup>) at 25°C ± 2°C. Intraparticle diffusion of adsorption of AY11 dye of initial concentration (75–200 mg L<sup>-1</sup>) by (d) Melon-B adsorbent dose (2.0 g L<sup>-1</sup>); of initial concentration (100–300 mg L<sup>-1</sup>) by (e) Melon-BO-NH<sub>2</sub>, and (f) Melon-BO-TETA adsorbent dose (2.0 g L<sup>-1</sup>) at 25°C ± 2°C.

Table 7

Elovich and intraparticle diffusion models results of adsorption of AY11 dye of different initial concentration (75–200 mg L<sup>-1</sup>) onto Melon-B of different adsorbent doses (2–6 g L<sup>-1</sup> dye solution) at 25°C ± 2°C

Melon-B dose (g L <sup>-1</sup> )	AY11 initial conc. (mg L <sup>-1</sup> )	Elovich			Intraparticle diffusion		
		$\beta$	$\alpha$	$R^2$	$K_{dif}$	C	$R^2$
2.0	75	0.25	117.95	0.990	1.15	20.31	0.989
	100	0.16	9.28	0.992	1.82	13.42	0.982
	150	0.10	13.64	0.992	2.64	15.66	0.991
	200	0.10	39.17	0.991	1.86	37.90	0.995
3.0	75	0.31	31.50	0.987	0.93	13.27	0.935
	100	0.25	9.34	0.973	1.20	10.33	0.999
	150	0.13	7.98	0.995	2.18	13.50	0.991
	200	0.13	50.33	0.958	2.29	27.56	0.991
4.0	75	0.50	153.49	0.963	0.56	12.40	0.882
	100	0.28	11.18	0.986	1.05	10.26	0.998
	150	0.19	11.49	0.979	1.53	13.06	0.998
	200	0.16	25.78	0.972	1.88	19.82	0.993
5.0	75	0.66	216.56	0.958	0.42	10.26	0.872
	100	0.45	101.05	0.988	0.63	12.43	0.941
	150	0.21	8.11	0.991	1.36	10.66	0.994
	200	0.19	35.94	0.996	1.55	19.72	0.971
6.0	75	0.95	1,071.25	0.945	0.29	9.19	0.853
	100	0.57	133.77	0.969	0.49	10.75	0.909
	150	0.38	184.14	0.991	0.75	16.04	0.939
	200	0.22	35.24	0.999	1.31	17.36	0.990

Table 8

Elovich and intraparticle diffusion models results of adsorption of AY11 dye of different initial concentration (100–300 mg L<sup>-1</sup>) onto Melon-BO-NH<sub>2</sub> of different adsorbent doses (0.5–2.0 g L<sup>-1</sup> dye solution) at 25°C ± 2°C

Melon-BO-NH <sub>2</sub> dose (g L <sup>-1</sup> )	AY11 initial conc. (mg L <sup>-1</sup> )	Elovich			Intraparticle diffusion		
		$\beta$	$\alpha$	$R^2$	$K_{dif}$	C	$R^2$
0.50	100	0.03	1.86E+01	0.971	10.89	39.41	0.955
	150	0.01	8.12E+00	0.970	21.88	-36.36	0.954
	200	0.01	7.52E+00	0.970	31.61	-101.29	0.952
	300	0.01	1.19E+01	0.903	31.64	-49.73	0.846
1.00	100	0.15	1.04E+05	0.980	1.89	74.07	0.979
	150	0.06	8.22E+02	0.966	4.62	89.34	0.981
	200	0.03	5.23E+01	0.978	9.50	71.26	0.991
	300	0.01	1.38E+01	0.978	21.85	3.09	0.985
1.25	100	0.43	7.68E+12	0.954	0.67	70.51	0.954
	150	0.14	5.38E+05	0.969	2.09	92.47	0.982
	200	0.06	8.28E+02	0.978	4.96	94.87	0.992
	300	0.02	2.46E+01	0.979	14.04	51.07	0.983
1.50	100	0.53	1.73E+13	0.969	0.54	59.11	0.965
	150	0.52	1.82E+20	0.970	0.56	91.75	0.967
	200	0.16	6.43E+07	0.975	1.80	109.65	0.991
	300	0.05	9.99E+02	0.975	6.34	119.31	0.997
2.00	100	0.73	3.71E+13	0.964	0.40	44.49	0.957
	150	0.65	6.74E+18	0.974	0.45	68.67	0.967
	200	0.29	4.01E+10	0.973	1.02	86.42	0.987
	300	0.11	8.22E+05	0.964	2.59	115.87	0.985

Table 9

Elovich and intraparticle diffusion models results of adsorption of AY11 dye of different initial concentration (100–300 mg L<sup>-1</sup>) onto Melon-BO-TETA of different adsorbent doses (0.5–2.0 g L<sup>-1</sup> dye solution) at 25°C ± 2°C

Melon-BO-TETA dose (g L <sup>-1</sup> )	AY11 initial conc. (mg L <sup>-1</sup> )	Elovich			Intraparticle diffusion		
		$\beta$	$\alpha$	$R^2$	$K_{dif}$	C	$R^2$
0.50	100	0.03	1.05E+01	0.993	10.54	18.65	0.972
	150	0.04	5.13E+02	0.968	7.04	116.12	0.963
	200	0.02	6.66E+01	0.852	12.67	105.81	0.726
	300	0.08	6.38E+09	0.917	3.67	265.40	0.977
1.00	100	0.05	1.01E+01	0.995	5.51	21.43	0.975
	150	0.10	3.49E+03	0.971	2.96	78.21	0.944
	200	0.11	4.43E+05	0.747	2.61	117.37	0.689
	300	0.08	1.86E+06	0.791	3.66	177.75	0.739
1.25	100	0.07	1.64E+01	0.981	3.84	27.21	0.916
	150	0.14	2.70E+04	0.970	2.13	72.11	0.988
	200	0.10	1.02E+04	0.971	2.82	87.16	0.912
	300	0.55	2.54E+40	0.049	0.19	172.45	0.007
1.50	100	0.07	1.04E+01	0.995	3.90	20.48	0.961
	150	0.13	2.09E+03	0.981	2.32	57.49	0.999
	200	0.08	1.01E+03	0.983	3.66	76.25	0.998
	300	1.57	1.73E+97	0.007	-0.02	145.49	0.000
2.00	100	0.11	1.24E+01	0.968	2.60	19.48	0.898
	150	0.13	8.54E+02	0.972	2.13	49.13	0.920
	200	0.15	1.02E+04	0.840	1.85	61.40	0.754
	300	0.91	1.89E+48	0.386	0.33	124.21	0.406

where C is the thickness of the boundary layer and  $K_{dif}$  is the intra-particle diffusion rate constant which directly evaluated from the intercept and the slope of the regression line, respectively. Parameters of the model for adsorption of AY11 dye by Melon-B, Melon-BO-NH<sub>2</sub>, and Melon-BO-TETA biochars are represented in Tables 7–9. Fig. 11d–f show the Webber–Morris adsorption line of AY11 dye adsorption onto the three biochars at different initial dye concentrations and different adsorbents dose. Since, the intraparticle diffusion curve does not pass through the origin point, which interpreted as the intraparticle diffusion is not rate determined.

#### 4. Conclusion

The above study shows that the biochar product derived from watermelon peels (Melon-B) was successfully modified with O<sub>3</sub> to produce the oxidized-biochar (Melon-BO) and then modified by two different amines such as ammonium hydroxide and triethylenetetramine to produce Melon-BO-NH<sub>2</sub> and Melon-BO-TETA biochars which were enriched with surface amino functional groups. Also, this study aimed to determine the effectiveness of non-commercial unmodified and modified biochars as a new type of adsorbent with high efficiency for the removal of AY11 dye from water using batch experimental methods at room temperature. The data presented in this work showed that both the NH<sub>4</sub>OH and the TETA reagents strongly influence the physicochemical properties of the biochars. In particular, an increase in the surface amino functional groups improved the adsorption process which strongly depended on the

level of these amino-containing moieties. On the basis of these observations, the electrostatic attraction force might be the primary mechanism controlling the adsorption of AY11 dye onto the biochars. Experimental results showed that the contact time necessary for maximum adsorption was 180 min and changing in pH values showed higher adsorption at acidic pH (1.0). Melon-B, Melon-BO-NH<sub>2</sub>, and Melon-BO-TETA biochars showed high adsorption capacity; 76.94, 445.48, and 462.18 mg g<sup>-1</sup>, respectively. The percentages of removal of AY11 dye were found to be 99%, 98%, and 96 % for Melon-B, Melon-BO-NH<sub>2</sub>, and Melon-BO-TETA biochars, respectively. Adsorption kinetics was found to follow the pseudo-second-order rate expression. Equilibrium adsorption data for AY11 dye on Melon-B and Melon-BO-NH<sub>2</sub> biochars were best represented by Freundlich isotherm. The Langmuir isotherm is the best-fit isotherm model for the experimental data of Melon-BO-TETA biochar. The modified biochars are considered as promising new adsorbents, cheaper adsorbent material, and an attractive option for effective removal of AY11 dye from wastewater or dilute industrial effluents to solve an environmental pollutant problem.

#### References

- [1] A. El Nemr, Impact, Monitoring & Management of Environmental Pollution, Nova Science Publishers, Inc., Hauppauge, New York, 2011, 638 pages.
- [2] M.A. Hassaan, A. El Nemr, Health and environmental impacts of dyes: mini review, Am. J. Environ. Sci. Eng., 1 (2017) 64–67.

- [3] A. El Nemr, Ed., Textiles: Types, Uses and Production Methods, Nova Science Publishers, Inc., Hauppauge, New York, 2012, 621 pages.
- [4] K. Nihan, Y. Zeynep, C. Selim, Preparation and characterization of biochar from hazelnut shell and its adsorption properties for methylene blue dye, *J. Polytech.*, 21 (2018) 765–776.
- [5] A. El Nemr, Ed., Non-Conventional Textile Waste Water Treatment, Nova Science Publishers, Inc., Hauppauge, New York, 2012, 267 pages.
- [6] S. Chakraborty, S. Chowdhury, P.D. Saha, Adsorption of crystal violet from aqueous solution onto NaOH-modified rice husk, *Carbohydr. Polym.*, 86 (2011) 1533–1541.
- [7] L. Wang, Y.Y. Yao, L.J. Sun, Y.J. Mao, W.Y. Lu, S.Q. Huang, W.X. Chen, Rapid removal of dyes under visible irradiation over activated carbon fibers supported Fe(III)-citrate at neutral pH, *Sep. Purif. Technol.*, 122 (2014) 449–455.
- [8] Y. Liu, D.-l. Xu, P. Wang, Y.-h. Dong, Removal of sodium salts and chemical oxygen demand from real reactive dye wastewater by the integrated process of chemical precipitation and extraction, *Desal. Water Treat.*, 57 (2016) 6772–6780.
- [9] E.T. Helmy, A. El Nemr, M. Mousa, E. Arafa, S. Eldafrawy, Photocatalytic degradation of organic dyes pollutants in the industrial textile wastewater by using synthesized TiO<sub>2</sub>, C-doped TiO<sub>2</sub>, S-doped TiO<sub>2</sub> and C,S co-doped TiO<sub>2</sub> nanoparticles, *J. Water Environ. Nanotechnol.*, 3 (2018) 116–127.
- [10] A. El Nemr, E.T. Helmy, E.A. Gomaa, S. Eldafrawy, M. Mousa, Photocatalytic and biological activities of undoped and doped TiO<sub>2</sub> prepared by green method for water treatment, *J. Environ. Chem. Eng.*, 7 (2018) 103385.
- [11] M.A. Hassaan, M. El Katory, R.M. Ali, A. El Nemr, Photocatalytic degradation of reactive black 5 using photo-Fenton and ZnO nanoparticles under UV irradiation, *Egypt. J. Chem.*, 63 (2020) 1443–1459.
- [12] S. Dalhatou, C. Pétrier, S. Laminsi, S. Baup, Sonochemical removal of naphthol blue black azo dye: influence of parameters and effect of mineral ions, *Int. J. Environ. Sci. Technol.*, 12 (2015) 35–44.
- [13] A. Mishra, M. Bajpai, The flocculation performance of Tamarindus mucilage in relation to removal of vat and direct dyes, *Bioresour. Technol.*, 97 (2006) 1055–1059.
- [14] M. Chiappisi, M. Simon, M. Gradzielski, Toward bioderived intelligent nanocarriers for controlled pollutant recovery and pH-sensitive binding, *ACS Appl. Mater. Interfaces*, 7 (2015) 6139–6145.
- [15] S.J. Deng, R. Wang, H.J. Xu, X.S. Jiang, J. Yin, Hybrid hydrogels of hyperbranched poly(ether amine)s (hPEAs) for selective adsorption of guest molecules and separation of dyes, *J. Mater. Chem.*, 22 (2012) 10055–10061.
- [16] A. Thiam, I. Sirés, J.A. Garrido, R.M. Rodríguez, E. Brillas, Effect of anions on electrochemical degradation of azo dye Carmoisine (Acid Red 14) using a BDD anode and air-diffusion cathode, *Sep. Purif. Technol.*, 140 (2015) 43–52.
- [17] A. El Nemr, A. El-Sikaily, A. Khaled, O. Abdelwahab, Removal of toxic chromium from aqueous solution, wastewater and saline water by marine red alga *Pterocladia capillacea* and its activated carbon, *Arabian J. Chem.*, 8 (2015) 105–117.
- [18] A. El Nemr, O. Abdelwahab, A. El-Sikaily, A. Khaled, Removal of direct blue-86 from aqueous solution by new activated carbon developed from orange peel, *J. Hazard. Mater.*, 161 (2009) 102–110.
- [19] A. Khaled, A. El Nemr, A. El-Sikaily, O. Abdelwahab, Removal of Direct N Blue-106 from artificial textile dye effluent using activated carbon from orange peel: adsorption isotherm and kinetic studies, *J. Hazard. Mater.*, 165 (2009) 100–110.
- [20] S. Demierege, A. Toptas, E.M. Ayan, I. Yasa, J. Yanik, Removal of textile dyes from aqueous solutions by biosorption on mushroom stump wastes, *Chem. Ecol.*, 31 (2015) 365–378.
- [21] A.A. Kadam, H.S. Lade, D.S. Lee, S.P. Govindwar, Zinc chloride as a coagulant for textile dyes and treatment of generated dye sludge under the solid state fermentation: hybrid treatment strategy, *Bioresour. Technol.*, 176 (2015) 38–46.
- [22] M. Punzi, A. Anbalagan, R.A. Börner, B.-M. Svensson, M. Jonstrup, B. Mattiasson, Degradation of a textile azo dye using biological treatment followed by photo-Fenton oxidation: evaluation of toxicity and microbial community structure, *Chem. Eng. J.*, 270 (2015) 290–299.
- [23] D.R. Manenti, P.A. Soares, A.N. Módenes, F.R. Espinoza-Quiñones, R.A.R. Boaventura, R. Bergamasco, V.J.P. Vilar, Insights into solar photo-Fenton process using iron(III)-organic ligand complexes applied to real textile wastewater treatment, *Chem. Eng. J.*, 266 (2015) 203–212.
- [24] Q. Chen, Y. Yang, M. Zhou, M.H. Liu, S.C. Yu, C.J. Gao, Comparative study on the treatment of raw and biologically treated textile effluents through submerged nanofiltration, *J. Hazard. Mater.*, 284 (2015) 121–129.
- [25] M. Ahmad, S.S. Lee, X.M. Dou, D. Mohan, J.-K. Sung, J.E. Yang, Y.S. Ok, Effects of pyrolysis temperature on soybean stover- and peanut shell-derived biochar properties and TCE adsorption in water, *Bioresour. Technol.*, 118 (2012) 536–544.
- [26] C. Raghavacharya, Colour removal from industrial effluents a comparative review of available technologies, *Chem. Eng. World*, 32 (1997) 53–54.
- [27] V.K. Gupta, R. Jain, S. Varshney, Electrochemical removal of the hazardous dye Reactofix Red 3 BFN from industrial effluents, *J. Colloid Interface Sci.*, 312 (2007) 292–296.
- [28] S.H. Lin, C.F. Peng, Treatment of textile wastewater by electrochemical method, *Water Res.*, 28 (1994) 277–282.
- [29] A. El Nemr, M.A. Hassaan, F.F. Madkour, Advanced oxidation process (AOP) for detoxification of acid red 17 dye solution and degradation mechanism, *Environ. Process.*, 5 (2018) 95–113.
- [30] M.A. Hassaan, A. El Nemr, F.F. Madkour, Testing the advanced oxidation processes on the degradation of Direct Blue 86 dye in wastewater, *Egypt. J. Aquat. Res.*, 43 (2017) 11–19.
- [31] M.A. Hassaan, A. El Nemr, F.F. Madkour, Advanced oxidation processes of Mordant Violet 40 dye in freshwater and seawater, *Egypt. J. Aquat. Res.*, 43 (2017) 1–9.
- [32] M. Rafatulla, O. Sulaiman, R. Hashim, A. Ahmad, Adsorption of methylene blue on low-cost adsorbents: a review, *J. Hazard. Mater.*, 177 (2010) 70–80.
- [33] N.S. Shah, J.A. Khan, M. Sayed, Z. Ul Haq Khan, J. Iqbal, S. Arshad, M. Junaid, H.M. Khan, Synergistic effects of H<sub>2</sub>O<sub>2</sub> and S<sub>2</sub>O<sub>8</sub><sup>2-</sup> in the gamma radiation induced degradation of congo-red dye: kinetics and toxicities evaluation, *Sep. Purif. Technol.*, 233 (2020) 115966.
- [34] J. Mohanraj, D. Durgalakshmi, S. Balakumar, P. Aruna, S. Ganesan, S. Rajendran, Mu. Naushad, Low cost and quick time absorption of organic dye pollutants under ambient condition using partially exfoliated graphite, *J. Water Process Eng.*, 34 (2020) 101078.
- [35] Mu. Naushad, G. Sharma, Z.A. Alothman, Photodegradation of toxic dye using Gum Arabic-crosslinked-poly(acrylamide)/Ni(OH)<sub>2</sub>/FeOOH nanocomposites hydrogel, *J. Cleaner Prod.*, 241 (2019) 118263.
- [36] G. Sharma, A. Kumar, Mu. Naushad, A. Kumar, A.H. Al-Muhtaseb, P. Dhiman, A.A. Ghfar, F.J. Stadler, M.R. Khan, Photoremediation of toxic dye from aqueous environment using monometallic and bimetallic quantum dots based nanocomposites, *J. Cleaner Prod.*, 172 (2018) 2919–2930.
- [37] D.K. Mahmoud, M.A.M. Salleh, W.A.W.A. Karim, A. Idris, Z.Z. Abidin, Batch adsorption of basic dye using acid treated kenaf fibre char: equilibrium, kinetic and thermodynamic studies, *Chem. Eng. J.*, 181 (2012) 449–457.
- [38] Y.P. Qiu, Z.Z. Zheng, Z.L. Zhou, G.D. Sheng, Effectiveness and mechanisms of dye adsorption on a straw-based biochar, *Bioresour. Technol.*, 100 (2009) 5348–5351.
- [39] R.-k. Xu, S.-c. Xiao, J.-h. Yuan, A.-z. Zhao, Adsorption of methyl violet from aqueous solutions by the biochars derived from crop residues, *Bioresour. Technol.*, 102 (2011) 10293–10298.
- [40] A.G.M. Shoaib, A. El-Sikaily, A. El Nemr, A.E.-D.A. Mohamed, A.A. Hassan, Preparation and characterization of highly surface area activated carbons followed Type IV from marine red alga (*Pterocladia capillacea*) by zinc chloride activation, *Biomass Convers. Biorefin.*, (2020) (in Press), <https://doi.org/10.1007/s13399-020-00760-8>.
- [41] D. Mohan, A. Sarswat, Y.S. Ok, C.U. Pittman Jr., Organic and inorganic contaminants removal from water with biochar,

- a renewable, low cost and sustainable adsorbent – a critical review, *Bioresour. Technol.*, 160 (2014) 191–202.
- [42] X.P. Gai, H.Y. Wang, J. Liu, L.M. Zhai, S. Liu, T.Z. Ren, H.B. Liu, Effects of feedstock and pyrolysis temperature on biochar adsorption of ammonium and nitrate, *PLoS One*, 9 (2014) 113888.
- [43] M.B. Ahmed, J.L. Zhou, H.H. Ngo, W.S. Guo, M.F. Chen, Progress in the preparation and application of modified biochar for improved contaminant removal from water and wastewater, *Bioresour. Technol.*, 214 (2016) 836–851.
- [44] S.J. Gregg, K.S.W. Sing, *Adsorption, Surface Area and Porosity*, 2nd ed., Academic Press, London, 1982.
- [45] F. Rouquerol, J. Rouquerol, K. Sing, *Adsorption by Powders and Porous Solids*, Academic Press, London, 1999.
- [46] E.P. Barrett, L.G. Joyner, P.P. Halenda, The determination of pore volume and area distributions in porous substances. I. Computations from nitrogen isotherms, *J. Am. Chem. Soc.*, 73 (1951) 373–380.
- [47] T. Madrakian, A. Afkhami, M. Ahmadi, H. Bagheri, Removal of some cationic dyes from aqueous solutions using magnetic-modified multi-walled carbon nanotubes, *J. Hazard. Mater.*, 196 (2011) 109–114.
- [48] J.W. Fu, Z.H. Chen, M.H. Wang, S.J. Liu, J.H. Zhang, J.N. Zhan, R.P. Han, Q. Xu, Adsorption of methylene blue by a high-efficiency adsorbent (polydopamine microspheres): kinetics, isotherm, thermodynamics and mechanism analysis, *Chem. Eng. J.*, 259 (2015) 53–61.
- [49] A. El Nemr, A. El-Sikaily, A. Khaled, Modeling of adsorption isotherms of Methylene Blue onto rice husk activated carbon, *Egypt. J. Aquat. Res.*, 36 (2010) 403–425.
- [50] I. Langmuir, The constitution and fundamental properties of solids and liquids. Part I. Solids, *J. Am. Chem. Soc.*, 38 (1916) 2221–2295.
- [51] A. El-Sikaily, A. El Nemr, A. Khaled, Copper sorption onto dried red alga *Pterocladia capillacea* and its activated carbon, *Chem. Eng. J.*, 168 (2011) 707–714.
- [52] H.M.F. Freundlich, Über die adsorption inlösungen, *Zeitschrift für Physikalische Chemie (Leipzig)*, 57A (1906) 385–470.
- [53] A. El Nemr, Potential of pomegranate husk carbon for Cr(VI) removal from wastewater: kinetic and isotherm studies, *J. Hazard. Mater.*, 161 (2009) 132–141.
- [54] M.J. Temkin, V. Pyzhev, Kinetics of ammonia synthesis on promoted iron catalysts, *Acta Physicochim. URSS*, 12 (1940) 217–222.
- [55] A. El Nemr, Pomegranate husk as an adsorbent in the removal of toxic chromium from wastewater, *Chem. Ecol.*, 23 (2007) 409–425.
- [56] A. El Nemr, M.M. El Sadaawy, A. Khaled, A. El Sikaily, Adsorption of the anionic dye Direct Red 23 onto new activated carbons developed from *Cynara cardunculus*: kinetics, equilibrium and thermodynamics, *Blue Biotechnol. J.*, 3 (2014) 121–142.
- [57] A. Eleryan, A. El Nemr, M. Mashaly, A. Khaled, 6-Triethylenetetramine 6-deoxycellulose grafted with crotonaldehyde as adsorbent for Cr<sup>6+</sup> removal from wastewater, *Int. J. Sci. Eng. Res.*, 10 (2019) 1199–1211.
- [58] J.F. Porter, G. McKay, K.H. Choy, The prediction of sorption from a binary mixture of acidic des using single-and mixed-isotherm variants of the ideal adsorbed solute theory, *Chem. Eng. Sci.*, 54 (1999) 5863–5885.
- [59] Y.-S. Ho, W.-T. Chiu, C.-C. Wang, Regression analysis for the sorption isotherms of basic dyes on sugarcane dust, *Bioresour. Technol.*, 96 (2005) 1285–1291.
- [60] S.J. Allen, Q. Gan, R. Matthews, P.A. Johnson, Comparison of optimized isotherm models for basic dye adsorption by kudzu, *Bioresour. Technol.*, 88 (2003) 143–152.
- [61] S. Lagergren, Zurtheorie der sogenannten adsorption gelösterstoffe, *Ungliga Svenska Vetenskaps akademien, Handlingar*, 24 (1898) 1–39.
- [62] Y.S. Ho, G. McKay, D.A.J. Wase, C.F. Foster, Study of the sorption of divalent metal ions on to peat, *Adsorpt. Sci. Technol.*, 18 (2000) 639–650.
- [63] J. Zeldowitsch, Über den mechanismus derkatalytischen oxidation von CO and MnO<sub>2</sub>, *Acta Physicochim. URSS*, 1 (1934) 364–449.
- [64] S.H. Chien, W.R. Clayton, Application of Elovich equation to the kinetics of phosphate release and sorption in soils, *Soil Sci. Soc. Am. J.*, 44 (1980) 265–268.
- [65] D.L. Sparks, *Kinetics of Reaction in Pure and Mixed Systems in Soil Physical Chemistry*, CRC Press, Boca Raton, 1986.
- [66] W.J. Weber, J.C. Morris, Kinetics of adsorption on carbon from solution, *J. Sanit. Eng. Div. Am. Soc. Civ. Eng.*, 89 (1963) 31–60.
- [67] K. Srinivasan, N. Balasubramanian, T.V. Ramakrishan, Studies on chromium removal by rice husk carbon, *Ind. J. Environ. Health*, 30 (1988) 376–387.

## Supplementary information

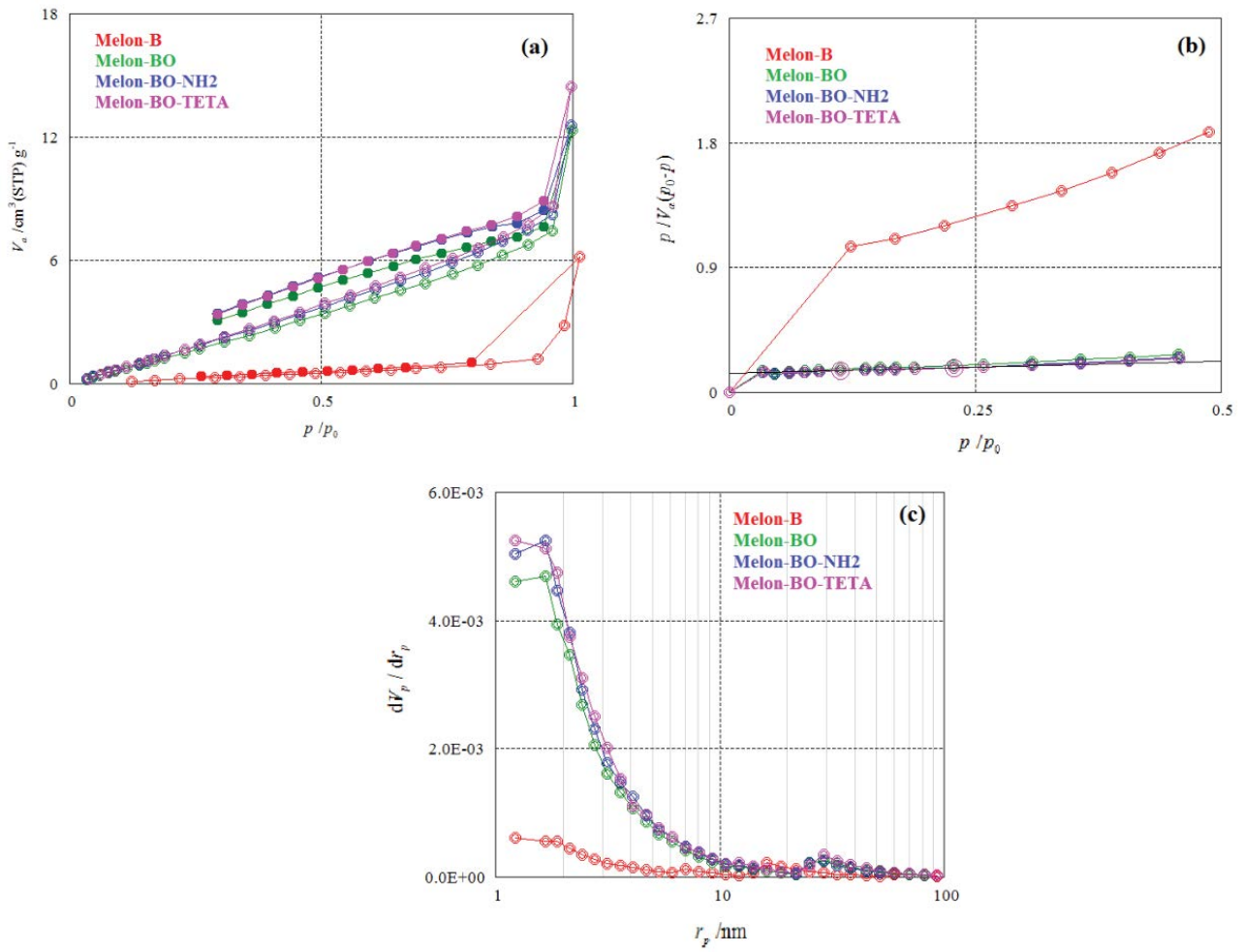


Fig. S1. (a) Adsorption-desorption, (b) BET analysis, and (c) BJH analysis plot of Melon-B, Melon-BO, Melon-BO-NH<sub>2</sub>, and Melon-BO-TETA biochars.

Table S1

The relation between  $q_e$  (mg g<sup>-1</sup>) of Acid Yellow 11 (AY11) dye at different initial concentrations (75, 100, 150, and 200 mg L<sup>-1</sup>) obtained by batch experimental and  $q_e$  (mg g<sup>-1</sup>) calculated using data obtained from different isotherm models using different doses of Melon-B (2–6 g L<sup>-1</sup>) at 25°C ± 2°C

Isotherm			Langmuir	Freundlich	Temkin	Dubinin–Radushkevitch isotherm
Melon-B dose (g L <sup>-1</sup> )	Initial conc. (mg L <sup>-1</sup> )	$q_{e,exp.}$ (mg g <sup>-1</sup> )	$q_{e,calc.}$ (mg g <sup>-1</sup> )			
2.0	75	35.74	23.91	33.70	31.74	59.5
	100	43.57	49.55	48.11	50.18	59.5
	150	58.06	66.19	62.79	63.99	59.5
	200	76.94	70.02	68.35	68.39	59.5
3.0	75	24.26	23.62	24.53	24.98	43.2
	100	28.40	40.19	41.53	43.72	43.2
	150	43.66	41.33	44.52	46.20	43.2
	200	61.92	39.99	41.08	43.34	43.2
4.0	75	18.39	16.12	17.92	16.88	36.8
	100	24.10	27.05	25.36	26.99	36.8
	150	34.47	39.41	40.06	40.30	36.8
	200	47.08	39.12	39.49	39.88	36.8
5.0	75	14.72	23.09	22.32	23.78	26.2
	100	19.94	10.72	16.78	16.50	26.2
	150	28.28	30.42	30.69	31.92	26.2
	200	38.95	29.24	28.11	29.68	26.2
6.0	75	12.27	20.35	20.76	22.27	22.1
	100	16.64	4.76	14.41	13.57	22.1
	150	24.75	21.11	21.05	22.61	22.1
	200	32.50	30.88	26.08	27.72	22.1

Table S2

The relation between  $q_e$  (mg g<sup>-1</sup>) of AY11 dye at different initial concentrations (100, 150, 200, and 300 mg L<sup>-1</sup>) obtained by batch experimental and  $q_e$  (mg g<sup>-1</sup>) calculated using data obtained from different isotherm models using different doses of Melon-BO-NH<sub>2</sub> (0.5, 1.0, 1.25, 1.50, and 2.00 g L<sup>-1</sup> dye solution) at 25°C ± 2°C

Isotherm		Langmuir	Freundlich	Temkin	Dubinin–Radushkevitch isotherm	
Melon-BO-NH <sub>2</sub> dose (g L <sup>-1</sup> )	Initial conc. (mg L <sup>-1</sup> )	$q_{e,exp.}$ (mg g <sup>-1</sup> )	$q_{e,calc.}$ (mg g <sup>-1</sup> )			
0.50	100	188.50	147.94	185.97	182.19	354.83
	150	284.13	289.18	271.77	295.31	355.04
	200	354.75	362.78	331.79	354.81	355.06
	300	445.48	442.15	442.31	440.55	355.06
1.00	100	98.75	72.41	97.67	92.21	211.87
	150	146.36	147.43	143.48	155.74	212.01
	200	215.41	228.98	210.70	219.23	212.04
	300	260.93	262.91	260.44	254.25	212.04
1.25	100	79.36	64.96	80.14	73.93	181.80
	150	118.41	120.25	115.56	127.68	181.91
	200	156.45	174.93	159.12	174.66	181.93
	300	231.03	225.32	230.36	228.98	181.94
1.50	100	56.33	54.48	65.43	43.92	156.41
	150	99.05	109.88	103.49	105.22	156.50
	200	131.82	139.86	127.78	133.40	156.51
	300	196.05	194.18	196.16	190.70	156.52
2.00	100	49.77	47.17	53.26	49.05	127.76
	150	74.57	71.89	69.28	73.11	127.82
	200	99.06	106.64	96.29	103.23	127.85
	300	147.18	145.79	152.34	145.20	127.87

Table S3

The relation between  $q_e$  (mg g<sup>-1</sup>) of AY11 dye at different initial concentrations (100, 150, 200, and 300 mg L<sup>-1</sup>) obtained by batch experimental and  $q_e$  (mg g<sup>-1</sup>) calculated using data obtained from different isotherm models using different doses of Melon-BO-TETA (0.5–2.0 g L<sup>-1</sup>) at 25°C ± 2°C

Isotherm		Langmuir	Freundlich	Temkin	Dubinin–Radushkevitch isotherm	
Melon-BO-TETA dose(g L <sup>-1</sup> )	Initial conc. (mg L <sup>-1</sup> )	$q_{e,exp.}$ (mg g <sup>-1</sup> )	$q_{e,calc.}$ (mg g <sup>-1</sup> )			
0.50	100	183.09	187.60	183.84	155.92	337.27
	150	290.44	297.73	275.55	301.94	337.46
	200	352.66	320.61	314.51	349.67	337.47
	300	462.18	332.16	359.36	397.77	337.48
1.00	100	94.41	100.78	94.98	75.72	208.79
	150	140.41	132.97	134.08	133.85	208.90
	200	180.12	163.99	160.17	163.82	208.93
	300	274.30	194.90	273.18	253.83	208.96
1.25	100	75.94	81.43	79.78	79.97	194.46
	150	113.46	112.65	110.70	114.75	194.57
	200	140.17	139.14	141.90	141.12	194.61
	300	213.43	213.99	290.26	217.12	194.64
1.50	100	88.30	110.29	33.03	86.00	201.07
	150	95.02	111.11	42.72	93.62	201.12
	200	127.68	117.86	54.93	101.06	201.15
	300	177.45	177.02	157.05	181.74	201.27
2.00	100	70.04	70.66	87.88	46.17	239.36
	150	78.53	78.05	110.97	66.13	239.44
	200	94.41	94.53	170.83	103.03	239.55
	300	133.07	113.74	259.31	138.72	239.62